OPEN ACCESS



S⁵: The Orbital and Chemical Properties of One Dozen Stellar Streams

Ting S. Li^{1,2,3,23}, Alexander P. Ji^{4,5}, Andrew B. Pace⁶, Denis Erkal⁷, Sergey E. Koposov^{8,9,10}, Nora Shipp^{4,5,11}, Gary S. Da Costa^{12,13}, Lara R. Cullinane¹², Kyler Kuehn^{14,15}, Geraint F. Lewis¹⁶, Dougal Mackey¹²,

```
Jeffrey D. Simpson<sup>13,17</sup>, Daniel B. Zucker<sup>18,19</sup>, Peter S. Ferguson<sup>20</sup>, Sarah L. Martell<sup>13,17</sup>, Joss Bland-Hawthorn<sup>13,16</sup>, Eduardo Balbinot<sup>21</sup>, Kiyan Tavangar<sup>4,5</sup>, Alex Drlica-Wagner<sup>4,5,22</sup>, Gayandhi M. De Silva<sup>13,15</sup>, and Joshua D. Simon<sup>2</sup>
                                                                            (S<sup>5</sup> Collaboration)
       Department of Astronomy and Astrophysics, University of Toronto, 50 St. George Street, Toronto ON, M5S 3H4, Canada; ting.li@astro.utoronto.ca
                              Observatories of the Carnegie Institution for Science, 813 Santa Barbara Street, Pasadena, CA 91101, USA
                                         Department of Astrophysical Sciences, Princeton University, Princeton, NJ 08544, USA
                         <sup>4</sup> Department of Astronomy & Astrophysics, University of Chicago, 5640 S Ellis Avenue, Chicago, IL 60637, USA
                                        Kavli Institute for Cosmological Physics, University of Chicago, Chicago, IL 60637, USA
                        <sup>6</sup> McWilliams Center for Cosmology, Carnegie Mellon University, 5000 Forbes Avenue, Pittsburgh, PA 15213, USA
                                                  Department of Physics, University of Surrey, Guildford GU2 7XH, UK
                           <sup>8</sup> Institute for Astronomy, University of Edinburgh, Royal Observatory, Blackford Hill, Edinburgh EH9 3HJ, UK
                                     Institute of Astronomy, University of Cambridge, Madingley Road, Cambridge CB3 0HA, UK
                               <sup>10</sup> Kavli Institute for Cosmology, University of Cambridge, Madingley Road, Cambridge CB3 0HA, UK
                                         MIT Kavli Institute for Astrophysics and Space Research, Cambridge, MA 02139, USA
                         <sup>12</sup> Research School of Astronomy and Astrophysics, Australian National University, Canberra, ACT 2611, Australia
                                       Centre of Excellence for All-Sky Astrophysics in Three Dimensions (ASTRO 3D), Australia
                                                 Lowell Observatory, 1400 W Mars Hill Road, Flagstaff, AZ 86001, USA
               Australian Astronomical Optics, Faculty of Science and Engineering, Macquarie University, Macquarie Park, NSW 2113, Australia
                               Sydney Institute for Astronomy, School of Physics, A28, The University of Sydney, NSW 2006, Australia
                                                          School of Physics, UNSW, Sydney, NSW 2052, Australia
                                     <sup>18</sup> Department of Physics & Astronomy, Macquarie University, Sydney, NSW 2109, Australia
                      <sup>19</sup> Macquarie University Research Centre for Astronomy, Astrophysics & Astrophotonics, Sydney, NSW 2109, Australia
                               Physics Department, University of Wisconsin-Madison, 1150 University Avenue, Madison, WI 53706, USA
                                  Kapteyn Instituut, Rijksunversiteit Groningen, Postbus 800, NL-9700AV Groningen, The Netherlands

<sup>22</sup> Fermi National Accelerator Laboratory, P.O. Box 500, Batavia, IL 60510, USA
```

Abstract

Received 2021 October 13; revised 2021 December 17; accepted 2021 December 26; published 2022 March 24

We report the kinematic, orbital, and chemical properties of 12 stellar streams with no evident progenitors using line-of-sight velocities and metallicities from the Southern Stellar Stream Spectroscopic Survey (S^5), proper motions from Gaia EDR3, and distances derived from distance tracers or the literature. This data set provides the largest homogeneously analyzed set of streams with full 6D kinematics and metallicities. All streams have heliocentric distances between ~10 and 50 kpc. The velocity and metallicity dispersions show that half of the stream progenitors were disrupted dwarf galaxies (DGs), while the other half originated from disrupted globular clusters (GCs), hereafter referred to as DG and GC streams. Based on the mean metallicities of the streams and the mass—metallicity relation, the luminosities of the progenitors of the DG streams range between those of Carina and Ursa Major I ($-9.5 \leq M_V \leq -5.5$). Four of the six GC streams have mean metallicities of [Fe/H] < -2, more metal poor than typical Milky Way (MW) GCs at similar distances. Interestingly, the 300S and Jet GC streams are the only streams on retrograde orbits in our dozen-stream sample. Finally, we compare the orbital properties of the streams with known DGs and GCs in the MW, finding several possible associations. Some streams appear to have been accreted with the recently discovered Gaia–Enceladus–Sausage system, and others suggest that GCs were formed in and accreted together with the progenitors of DG streams whose stellar masses are similar to those of Draco to Carina ($\sim 10^5 - 10^6 M_{\odot}$).

Unified Astronomy Thesaurus concepts: Local Group (929); Milky Way Galaxy (1054); Stellar streams (2166); Globular star clusters (656); Dwarf galaxies (416); Stellar kinematics (1608)

1. Introduction

The hierarchical model of galaxy formation posits that the Milky Way (MW) was assembled through the accretion and disruption of many smaller systems (Peebles 1965; Press &

Original content from this work may be used under the terms of the Creative Commons Attribution 4.0 licence. Any further distribution of this work must maintain attribution to the author(s) and the title of the work, journal citation and DOI.

Schechter 1974; Searle & Zinn 1978; Blumenthal et al. 1984), such as dwarf galaxies (DGs) and globular clusters (GCs). Systems disrupted relatively recently can manifest as stellar streams, which provide a snapshot of accretion that can be compared directly with theoretical models of structure formation (e.g., Johnston 1998; Freeman & Bland-Hawthorn 2002; Bullock & Johnston 2005) and bridge the gap between the smooth stellar halo and the present-day MW satellite population. Furthermore, the spatial and kinematic properties of stellar streams are sensitive to the mass and three-dimensional shape of the MW's gravitational field (e.g., Koposov et al. 2010;

²³ NHFP Einstein Fellow.

Erkal et al. 2016b; Bovy et al. 2016; Bonaca & Hogg 2018). Gaps and kinks in stellar streams can also reveal the existence of low-mass dark matter substructure throughout the halo (e.g., Ibata et al. 2002; Johnston et al. 2002; Carlberg 2009; Varghese et al. 2011; Erkal et al. 2016a), a key prediction of the cold dark matter model.

As a result of the various ground-based photometric surveys in the past two decades, as well as the recent Gaia data releases. the number of known MW stellar streams has increased substantially to over 60 (e.g., Grillmair & Carlin 2016; Shipp et al. 2018; Mateu et al. 2018; Ibata et al. 2019). Some of these streams clearly emanate from known DGs or GCs (e.g., the Sagittarius and Palomar 5 streams), but most streams lack an obvious progenitor. While imaging surveys can provide on-sky positions, distances, and proper motions (PMs), spectroscopic observations can reveal line-of-sight velocities and chemical properties of the streams. However, spectroscopic observations of individual stars in stellar streams are extremely challenging due to the low stellar density and large angular extents (>10°) of these systems, particularly for the more distant (and thus fainter) streams beyond a heliocentric distance of 10 kpc. Prior to 2018, only a handful of stellar streams had spectroscopic measurements: Sagittarius (Majewski et al. 2003), Palomar 5 (Odenkirchen et al. 2009; Kuzma et al. 2015; Ibata et al. 2016; Li et al. 2017a), Cetus (Newberg et al. 2009; Koposov et al. 2012; Yam et al. 2013; Li et al. 2017a), GD-1 (Koposov et al. 2010; Li et al. 2017a), Orphan (Newberg et al. 2010; Casey et al. 2013, 2014; Li et al. 2017a), Ophiuchus (Sesar et al. 2015), and the 300 km s⁻¹ stream (hereafter 300S; Simon et al. 2011; Frebel et al. 2013; Fu et al. 2018). Even for these spectroscopically confirmed streams, spectroscopic measurements are often quite sparse due to the challenges of efficiently targeting member stars. This has made it hard to answer some of the most basic of questions, such as whether these streams originated from disrupting GCs or dissolving DGs.

The Southern Stellar Stream Spectroscopic Survey (S⁵; Li et al. 2019) was initiated in 2018 using the Two-degree Field (2dF) fiber positioner (Lewis et al. 2002) coupled with the dualarm AAOmega spectrograph (Sharp et al. 2006) on the 3.9 m Anglo-Australian Telescope (AAT). This ongoing survey pursues a complete census of known streams in the southern hemisphere and has so far produced observations of more than 20 stellar streams. In this paper, we present the most recent measurements of the stream properties for 12 stellar streams that have a robust detection of spectroscopic members from S° : ATLAS-Aliqa Uma (AAU), Elqui, Indus, Jet, Jhelum, Orphan-Chenab, Ophiuchus, Palca, Phoenix, Turranburra, Willka Yaku, and 300S. In addition, we also report the failure to detect spectroscopic stream members in the following stream candidates: Ravi, Wambelong, and Styx. Except for Ophiuchus at ~ 8 kpc, all of the streams we present here are distant, with heliocentric distances between 10 and 50 kpc. This is currently the largest homogeneously analyzed set of streams with full 6D kinematics and metallicities. Here we only focus on streams that have no obvious progenitors inside the streams, although S⁵ has also observed several streams with known progenitors (i.e., GCs or DGs presenting tidal tails, but which are not fully disrupted; e.g., Ji et al. 2021).

In Section 2, we describe the stream observables from the data, such as distance, velocity, and metallicities. In Section 3, we discuss the properties of the progenitors of these streams based on their kinematic and metallicity results from Section 2.

In Section 4, we discuss our findings based on the measurements, and we conclude in Section 5.

2. Data in 6+1D

2.1. S⁵ Data

The data used in this paper are from an internal S^5 data release (iDR3.1) where the analysis has been improved compared to Li et al. (2019, previously iDR1.5); S⁵ observations taken between 2018 and 2020 are included. For details of the updates in the spectral fitting, we refer readers to Ji et al. (2021). In short, we simultaneously model spectra from both the red and blue arms of AAOmega as well as repeated observations of the same object from different nights with rvspecfit (Koposov 2019), which provides radial velocities (RVs), effective temperatures ($T_{\rm eff}$), surface gravities (log g), stellar metallicities ([Fe/H]), and alpha abundance ([α /Fe]) estimates for each star. The blue spectra make the metallicities from ryspecfit more accurate than those for iDR1.5 (where metallicities were derived using only the spectra from the red arm). We also derived preliminary distance measurements for individual stars as the updates from iDR2.2 (used in Ji et al. 2021) to iDR3.1. The distances are determined using a full combination of parallax from Gaia, the spectra from S^5 , the available optical/infrared photometry for each star, and MIST isochrones (Choi et al. 2016). We estimate a distance uncertainty of ~25% for distant stars with poor parallax measurements from this spectrophotometric derivation, and we are actively working to improve the distance uncertainty for future releases.

We also determine calcium triplet (CaT) metallicities from equivalent widths (EWs) and the Carrera et al. (2013) calibration for all the red giant branch stream member stars. CaT metallicities are more accurate than those from rvspecfit when the distances to the stars are known (Li et al. 2019; Ji et al. 2020). EWs were measured by fitting a Gaussian plus Lorentzian function (e.g., Li et al. 2017b). A systemic uncertainty floor of 0.19 Å, computed from repeated observations, is added in addition to the covariance from the EW fit as the total uncertainty on the EW, and then transferred to the CaT metallicity uncertainty through error propagation using the Carrera et al. (2013) calibration relation. The absolute V magnitudes are determined from Gaia EDR3 G, Bp, and Rp photometry, first applying the color transformation function defined in Riello et al. (2021), then dereddening using Schlegel et al. (1998) and Schlafly & Finkbeiner (2011) and adding the distance moduli of individual stars detailed in Section 2.3.

2.2. Member Stars in 12 Streams

We report the kinematic and chemical properties of the following one dozen streams that were observed in S^5 between 2018 and 2020: AAU, Elqui, Indus, Jet, Jhelum, Orphan-Chenab, Ophiuchus, Palca, Phoenix, Turranburra, Willka Yaku, and 300S, most of which were first discovered in the Dark Energy Survey (DES; Shipp et al. 2018) using a matched filter in color–magnitude space derived from a synthetic isochrone of an old, metal-poor stellar population. The Sagittarius (Sgr) stream was also observed in S^5 , which we only show for comparison here given the numerous previous studies on Sgr (e.g., Hasselquist et al. 2019; Yang et al. 2019; Johnson et al. 2020). S^5 had not completed planned observations of 300S, Turranburra, Jet, Palca, and Orphan-Chenab by

the end of 2020, but enough data had been collected to allow member stars to be identified for this study.

Six of our streams have detailed membership studies published or in preparation. For streams with published S^5 papers, we take the spectroscopic members directly from the references (Li et al. 2021 for AAU and Palca; Wan et al. 2020 for Phoenix). These studies use Gaia DR2, but switching to EDR3 makes no difference to their membership. Detailed membership studies by S⁵ for Indus and Jhelum (A. B. Pace et al. 2022, in preparation) and Elqui (S. Martell et al. in preparation) are underway, so we use stars with high membership probabilities (P > 0.8) from those studies as stream members. The membership is computed using a probabilistic mixture model detailed in Wan et al. (2020). For Orphan-Chenab, we select member stars within ± 15 km s⁻¹ and ± 0.4 mas yr 1 from the best RV and PM track determined in S. E. Koposov et al. (2022, in preparation) through fitting to RV data from S^5 and other spectroscopic surveys as well as fitting for stream PM in Gaia EDR3 data, expanding the analysis from Koposov et al. (2019). Because parts of the stream have velocities close to MW foreground stars, we also require a heliocentric S^5 iDR3.1 distance larger than 10 kpc to remove foreground main-sequence stars. Note that Orphan and Chenab are a single stream (Koposov et al. 2019), but because the stream is extremely long (over 200° on the sky) and the southern part is heavily perturbed by the Large Magellanic Cloud (LMC; Erkal et al. 2019), we consider their properties separately to probe the possible kinematic and metallicity variation along the long stream. We define the Orphan and Chenab components of this stream as $\phi_1 > 0$ and $\phi_1 < 0$, respectively, with ϕ_1 as defined in Koposov et al. (2019).

For the remaining streams—i.e., Jet, Turranburra, 300S, Ophiuchus, and Willka Yaku—no comprehensive membership modeling has yet been performed. We select member stars with simple kinematic cuts using RVs from S⁵ and PMs from Gaia EDR3, using a similar method to that used for AAU in Li et al. (2021) and Phoenix in Wan et al. (2020), to ensure a sample that is as pure as possible. With the exception of Turranburra, all other likely stream members are selected only kinematically (so that no metallicity bias is introduced). Turranburra's kinematics are almost identical to foreground disk stars, so we select member stars with a metallicity criterion of [Fe/ H] < -1.5 to remove foreground stars. However, we believe that Turranburra is a real and distinct structure, given the low metallicities ([Fe/H] < -2) of most member stars. The member selection here is not the most comprehensive, but rather a straightforward and simple choice to (1) confirm that the stream is a real signature in kinematic and metallicity space, and (2) identify a list of high-purity (at a cost of lower completeness) members to study the kinematic, orbital, and metallicity properties of the stream for further discussion in later sections.

In Figure 1, we show the on-sky location of the spectroscopic members in the dozen streams that are used in this work. To ensure the quality of the data, we only include member stars with a signal-to-noise ratio (S/N) > 5 in red-arm spectra in this work, though S^5 does find more member stars at lower S/N. For individual stars, the typical uncertainties range from ~ 1 km s⁻¹ at S/N < 20 to ~ 4 km s⁻¹ at $S/N \sim 5$ for RV, and from 0.15 dex at S/N < 20 to 0.4 dex at $S/N \sim 5$ for metallicities. We refer readers to Li et al. (2019) for the reduction and validation of S^5 data. We also note that, as the observations in several streams have not yet finished, more

spectroscopic members are expected in future S^5 releases and publications.

2.3. Distance

Distance is a crucial input for both kinematic and chemical studies of these streams. Although S^5 iDR3.1 provides distances to individual stars, the uncertainties on individual stars are quite large (up to 25%). Therefore, in this work, we compute the stream distance measurements for all the streams that have DES photometry, using individual blue horizontal branch stars (BHBs) and RR Lyrae stars (RRLs), as described in Li et al. (2021).

BHB members are identified as spectroscopic stream members with g-r<0 that are not in the Gaia RRL catalogs (Clementini et al. 2019; Holl et al. 2018). The distance modulus of each BHB is calculated using the relation from Belokurov & Koposov (2016) and the dereddened DES DR2 photometry. We find RRL members by cross-matching spectroscopic members with the Gaia RRL catalogs. We then determine the distance moduli of the RRL stars using the relation from Muraveva et al. (2018),

$$M_G = 0.32 \, [\text{Fe/H}] + 1.11$$

and the dereddened Gaia G-band magnitudes, using the color-dependent extinction corrections from Gaia Collaboration et al. (2018) and E(B-V) values from Schlegel et al. (1998) and Schlafly & Finkbeiner (2011). Because the metallicities derived from the CaT EW require a distance input, we adopt a preliminary mean metallicity derived from BHB distances for the RRL distance derivation. We note that a 0.1 dex shift in metallicity will only impact the distance moduli by 0.03 mag for RRLs and is much smaller than the intrinsic dispersion of 0.17 mag found by Muraveva et al. (2018).

Among all the streams for which we have computed the distances with BHBs and RRLs, AAU has the most distance tracers, with 13 BHBs and 5 RRLs (Li et al. 2019). Other streams typically have several to a few (<10) BHBs and RRLs combined. We note that we only select BHB and RRL members from the spectroscopic sample. Therefore, more BHB and RRL members are likely present outside the AAT fields, especially for the streams with large stream widths, but we limit our selection to the stars that have line-of-sight velocities for a purer sample.

We then transfer all the BHB and RRL members into stream coordinates with the transformations defined in Shipp et al. (2019). If a distance gradient is obvious along the stream longitude ϕ_1 , we fit a first-order polynomial in ϕ_1 , which is useful for the orbital properties discussed later. Otherwise, we use a single average distance for the entire stream. The latter could be either due to a lack of distance gradient along the stream or a lack of distance tracers in the spectroscopic sample. We then assign a distance to each stream member based on the adopted relation. The adopted heliocentric distance relations and the average heliocentric distances to each stream are presented in Table 1. We note that all the updated distance relations here have a mean distance modulus no more than 0.1 mag different from Shipp et al. (2018), who computed the distance from isochrone fitting.

Our RRL sample might be incomplete, as the RRLs could have very large velocity variability and therefore might not be classified as spectroscopic members.

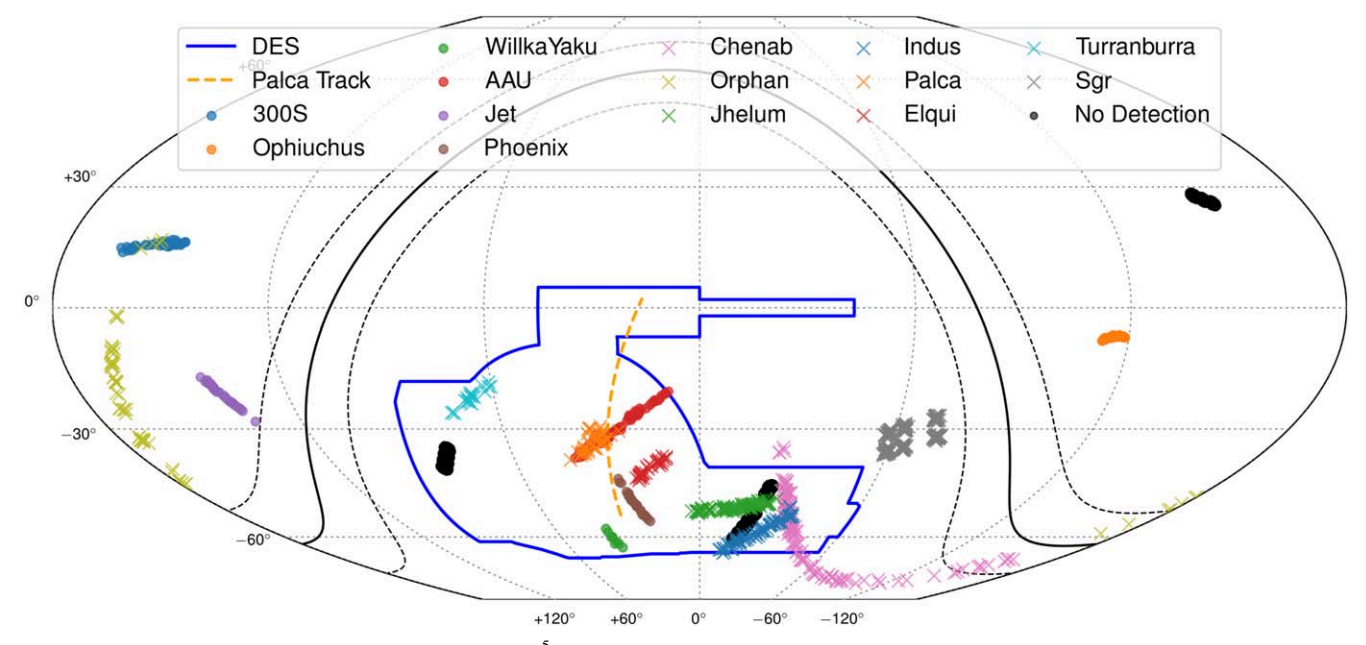


Figure 1. On-sky distribution of member stars identified with S^5 observations taken between 2018 and 2020 in a dozen stellar streams. Stars in streams that we consider to have had GC and DG progenitors are shown as circles and crosses, respectively. Among these streams, nine are within the DES footprint (outlined in blue). Three streams, Wambelong, Ravi, and Styx, have no clear spectroscopic members identified; the coverage by S^5 so far on these streams is shown in the black filled circles. Note that because no observations of Palca had been planned by S^5 , we have only identified Palca member stars in the AAU stream field (see Li et al. 2021 for more details). The Palca stream is much longer than the observed length, as indicated by the orange dashed line from Shipp et al. (2018).

DES photometry does not have full coverage for the following streams: Orphan-Chenab, 300S, Ophiuchus, Jet, and Sgr; we thus adopt the distances from a variety of references. For Orphan-Chenab, we take the distance track from S. E. Koposov et al. (2022, in preparation). The distances for 300S, Jet, and Ophiuchus are taken from the references listed in Table 1. For Sgr, we use the median distance from S^5 iDR3.1 for each Sgr field. Because there are a total of over 1000 member stars in Sgr stream fields, the median distance from S^5 iDR3.1 is sufficient to obtain Sgr's orbital properties.

2.4. Streams with No Detection of Spectroscopic Members

We failed to identify any clear member stars in the following three streams: Ravi, Wambelong, and Styx. Neither the Ravi nor Wambelong streams had conclusive PM signatures in Shipp et al. (2019) with Gaia DR2, and we cannot detect them in Gaia EDR3 with spectroscopic information either. Interestingly, the stream fields for both Ravi and Styx show groups of stars with small velocity dispersions that are known to belong to other structures. Specifically, member stars of the Tucana II DG are detected in the Ravi fields (at a much larger distance than Ravi's reported distance), and a group of Böotes III stars is detected in the Styx fields. These additional structures may have caused difficulties in finding member stars in these streams. Furthermore, the incomplete mapping of these streams may result in a failure to obtain spectroscopic confirmation. Only four out of seven Wambelong fields have been observed so far by S^5 ; Styx is a stream in the northern hemisphere and therefore we have only obtained three fields that are accessible from the AAT, and Ravi's stream fields largely overlap with those of the Jhelum and Indus streams. In Figure 1, we show the areas that have been covered by S^5 along these three streams as black shaded regions. Deeper data and/or larger surveyed areas are needed to confirm the reality of these

streams; alternatively, these streams might not be real structures.

3. Results

3.1. Velocities and Metallicities

After selecting all stream member stars, we use the RA, Dec, RVs, and [Fe/H] from S^5 for the individual member stars to determine the velocity dispersion, mean metallicity, and metallicity dispersion of each stream. Rather than fitting a comprehensive background model (which is carefully done in other S^5 papers), here we just take the dispersions from a high-purity sample of member stars directly.

For the velocity dispersion, we first fit the stream RVs as a function of ϕ_1 with a second-order polynomial and subtract that off as the systemic velocity of the stream along ϕ_1 . Then, we model the residual RV with a Gaussian distribution, including Gaussian velocity uncertainties on individual stars, to derive the velocity dispersion. The posterior on the velocity dispersion was derived with the Markov Chain Monte Carlo (MCMC) sampler <code>emcee</code> (Foreman-Mackey et al. 2013), similar to what has been done in kinematic studies of DGs (e.g., Li et al. 2017b). We use a uniform prior in log-space for the velocity dispersion with a prior range of $(0.01\text{--}100)\,\mathrm{km\,s^{-1}}$. The velocity dispersion of each stream is reported in Table 1.

Similarly, we derive the mean metallicity and metallicity dispersion of each stream assuming a Gaussian metallicity distribution function (independent of ϕ_1) with both the rvspecfit and CaT metallicities. For most of the streams, the mean metallicities from the two different methods (i.e., rvspecfit and CaT) give results consistent within 0.2 dex. The CaT metallicities are usually more accurate, though they rely on an accurate distance determination. As an example, the mean heliocentric distance of the 300S stream members is \sim 17 kpc from Fu et al. (2019); if we increased the distance by 30% to 22 kpc, then the mean metallicity of 300S would change

Stream	Distance ^a	$ar{d}_{\odot}$ (kpc)	σ_w^{b} (pc)	$N_{ m mem}$	$\sigma_{\text{vel}}^{\text{c}}$ (km s ⁻¹)	$N_{ m RGB}$	Fe/H] _{CaT}	$\sigma_{ m [Fe/H]}$	$\sigma_{ m [Fe/H]} \ (<95\%)$	Progenitor Type	Progenitor Analog
300S	$(d/1 \text{ kpc}) = 48.9952 - 0.2083\alpha$	17.2	110	53	$2.5^{+0.4}_{-0.3}$	52	$-1.26^{+0.03}_{-0.03}$	$0.04^{+0.04}_{-0.02}$	0.11	GC	
Ophiuchus	$\mu = 14.58 - 0.2(l - 5)$	7.9	8	118	$2.4^{+0.3}_{-0.3}$	37	$-1.80^{+0.03}_{-0.03}$	$0.03^{+0.03}_{-0.01}$	0.09	GC	
Willka Yaku	$\mu = 17.8$	36.3	127	9	$0.4^{+0.8}_{-0.4}$	7	$-2.05^{+0.07}_{-0.07}$	$0.04^{+0.07}_{-0.02}$	0.18	GC	
AAU	$\mu = 16.67 - 0.034\phi_1$	23.8	96	85	$4.3^{+0.4}_{-0.4}$	66	$-2.22^{+0.02}_{-0.02}$	$0.05^{+0.05}_{-0.03}$	0.13	GC	
Jet	$\mu = 17.45 - 0.014\phi_1$	30.4	90	32	$0.7^{+0.4}_{-0.5}$	29	$-2.38^{+0.03}_{-0.03}$	$0.04^{+0.05}_{-0.02}$	0.12	GC	
Phoenix	$\mu = 16.26 + 0.008\phi_1$	17.9	53	26	$2.5^{+0.7}_{-0.7}$	20	$-2.62^{+0.05}_{-0.05}$	$0.03^{+0.05}_{-0.02}$	0.13	GC	
Orphan	track from Koposov et al.	17.1	747	58	$4.1^{+0.5}_{-0.5}$	49	$-1.85^{+0.07}_{-0.07}$	$0.42^{+0.07}_{-0.06}$	0.53	DG	Leo II
Chenab	track from Koposov et al.	32.8	493	125	$4.5^{+0.5}_{-0.3}$	109	$-1.78^{+0.04}_{-0.04}$	$0.28^{+0.03}_{-0.03}$	0.34	DG	Leo II
Jhelum	$\mu = 15.4$	12.0	267	95	$13.7^{+1.2}_{-1.1}$	39	$-1.83^{+0.05}_{-0.05}$	$0.25^{+0.05}_{-0.04}$	0.34	DG	Leo II
Indus	$\mu = 15.90 - 0.016\phi_1$	15.2	240	75	$7.6_{-0.6}^{+0.7}$	66	$-1.96^{+0.05}_{-0.05}$	$0.33^{+0.05}_{-0.04}$	0.41	DG	Draco
Palca	$\mu = 17.8$	36.3	≥1000	42	$13.4^{+1.9}_{-1.4}$	32	$-2.02^{+0.04}_{-0.04}$	$0.13^{+0.06}_{-0.07}$	0.23	DG	Draco
Elqui	$\mu = 18.48 - 0.043\phi_1$	51.0	472	34	$16.2^{+2.3}_{-2.1}$	33	$-2.22^{+0.06}_{-0.06}$	$0.27^{+0.06}_{-0.05}$	0.37	DG	Ursa Major I
Turranburra	$\mu = 17.1$	26.3	288	22	$19.7^{+3.9}_{-3.0}$	15	$-2.18^{+0.13}_{-0.14}$	$0.39^{+0.12}_{-0.09}$	0.62	DG	Ursa Major I

Notes. As we probe the Orphan and Chenab components of the Orphan-Chenab stream separately, there are 13 rows for the 12 streams presented here. From left to right, the columns are the name of the stream, the distance relation adopted in this paper, average heliocentric distance \bar{d}_{\odot} , stream width σ_{w} , number of spectroscopic members in each stream, velocity dispersion σ_{vel} , number of red-giant branch members that have CaT metallicities, mean CaT metallicities $\overline{\text{[Fe/H]}}_{\text{CaT}}$, CaT metallicity dispersion $\sigma_{\text{[Fe/H]}}$, 95th percentile of the CaT metallicity dispersion, whether the progenitor is a dwarf galaxy (DG) or globular cluster (GC), and analogs to the known MW satellite galaxies based on their mean metallicities (if applicable), respectively.

S

^a Distance relation derived in this work with BHB and RRL members (see text for details) except for 300S (Fu et al. 2019; α is the R.A. of each star in degrees), Ophiuchus (Sesar et al. 2015, l is the Galactic longitude of each star in degrees), and Jet (Ferguson et al. 2022). For Orphan-Chenab, we adopt the distance relation from RRLs in S. E. Koposov et al. (2022, in preparation). For the Palca stream, the distance modulus is computed based on members at $(\alpha, \delta) = (33^{\circ}, -33^{\circ})$. Note that the distance for other parts of the stream may be different.

b Stream width, defined as one standard deviation of a Gaussian profile, taken from different literature, 300S (Fu et al. 2019), Ophiuchus (Bernard et al. 2014), Orphan (Grillmair 2006), and the rest from Shipp et al. (2018). Shipp et al. (2018) did not measure the width of the Palca stream. We therefore set it to be >1000 pc based on the measurements on the Cetus stream from Yam et al. (2013).

^c The velocity dispersion of Chenab and Orphan might be underestimated, as we selected member stars within $\pm 15~{\rm km~s^{-1}}$ from the RV track defined in S. E. Koposov et al. (in preparation) to minimize the background contamination. We refer to S. E. Koposov et al. (in preparation) for a more rigorous calculation.

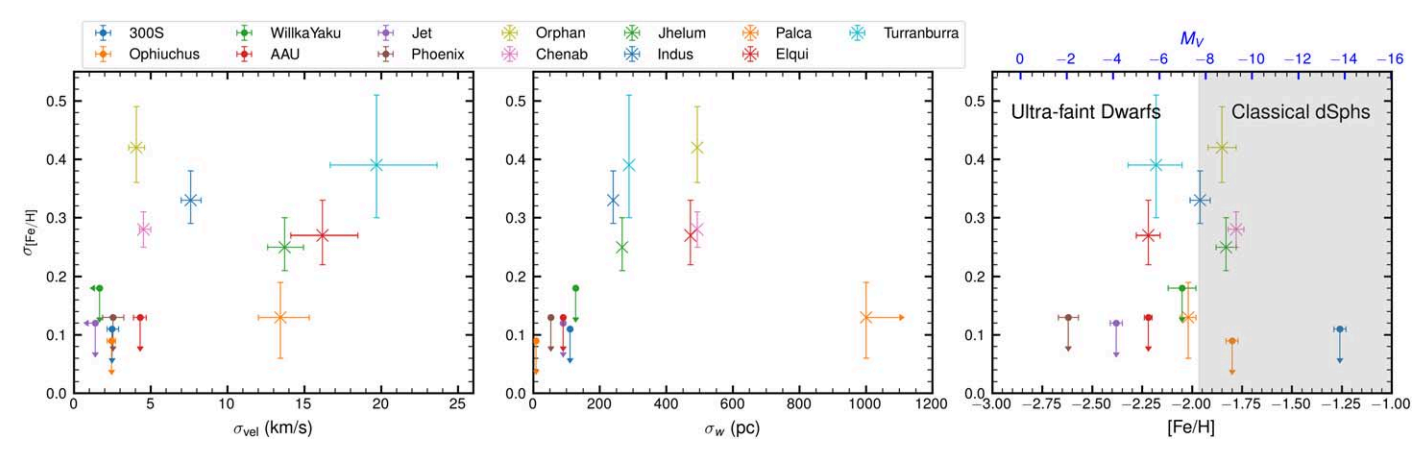


Figure 2. (Left) Velocity dispersion ($\sigma_{\rm vel}$) vs. metallicity dispersion ($\sigma_{\rm [Fe/H]}$) of one dozen streams. Six streams have both small velocity dispersions and metallicity dispersions and are classified as GC streams (circles); the other streams have larger metallicity dispersions and/or larger velocity dispersions and are classified as DG streams (crosses). If the dispersion is resolved, the median value is used for the symbol, and the errors are taken from the 16th and 84th percentiles. If the dispersion is not resolved, then the 95th percentile is used as the upper limit. (Middle) Stream width (σ_w) versus metallicity dispersion of one dozen streams. GC streams have smaller stream widths than DG streams. (right) Mean CaT metallicity ([Fe/H]) vs. metallicity dispersion for these streams. The top axis shows the corresponding luminosity for progenitors of the DG streams, based on the empirical luminosity—metallicity relation for intact DGs (Norris et al. 2010; Kirby et al. 2013b). $M_V = -7.7$ is used to separate classical dwarf spheroidals (dSphs) and ultrafaint dwarf (UFD) galaxies (Simon 2019).

from [Fe/H] = -1.27 (the mean value from the CaT measurements) to [Fe/H] = -1.4 (mean metallicity from rvspecfit).

Given the established membership of stars and thus well-known distances, we consider the metallicities and metallicity dispersions from CaT to be more accurate than those from rvspecfit. We therefore report the mean metallicities and metallicity dispersions of the dozen streams from the CaT metallicities in Table 1. Our metallicity discussion in Section 3.2 is also based on these quantities. Several streams have unresolved CaT metallicity dispersions, so we also give the 95% confidence upper limit on the metallicity dispersion in Table 1.

Finally, we note that the velocity dispersion of Orphan-Chenab might be biased low as $|\Delta RV| < 15 \text{ km s}^{-1}$ is used for the membership selection. Similarly, the mean metallicity and dispersion of Turranburra might be biased low because we discarded any possible member stars with |Fe/H| > -1.5.

3.2. Stream Progenitors

As shown in Table 1, of the 12 streams presented here, half show an unresolved CaT metallicity dispersion (i.e., the dispersion is consistent with zero within the 2σ uncertainty). Furthermore, these streams have metallicity dispersions below 0.2 dex at the 95% confidence level. We therefore conclude that the progenitors of these streams—i.e., 300S, AAU, Jet, Ophiuchus, Phoenix, and Willka Yaku—are likely to be GCs (hereafter referred to as GC streams). Most of these streams also show velocity dispersions below 3 km s⁻¹. AAU has a higher dispersion, likely as a result of heating via perturbations (Li et al. 2021). These six streams are all clustered in the lower-left corner in the left panel of Figure 2. We use circle symbols to represent streams (or stream members) whose progenitors are GCs throughout this paper.

The remaining six streams—Orphan-Chenab, Elqui, Indus, Palca, Turranbura, and Jhelum—show resolved metallicity dispersions, so their progenitors are likely to be DGs (hereafter referred to as DG streams). These streams also show larger velocity dispersions than the GC streams in general. In particular, four streams have unusually high velocity

dispersions of over $10~{\rm km\,s}^{-1}$ and are discussed in more detail in Section 4.5. We use cross symbols to represent DG streams (or stream members) throughout this paper. We note that, because the Palca stream was not targeted on purpose, the Palca members were selected with an isochrone selection at the distance of AAU ($\Delta {\rm DM} = 1.1$ closer than Palca). However, with a wide selection window in color and magnitude, most of the Palca members should be selected with the selection criteria for AAU. The brightest metal-rich members might be outside our selection window, which could result in a slightly lower metallicity dispersion.

Although the progenitor classification is primarily based on the metallicity dispersion, we see that both velocity dispersion and stream width also provide information about the progenitors. In the middle panel of Figure 2, we show the stream width 25 of the dozen streams, compiled from the literature. All of the GC streams have a stream width $\sigma_w < 150$ pc, while the DG streams have $\sigma_w > 200$ pc.

In the right panel of Figure 2, we show the mean metallicities of these streams. While the mean metallicities of the GC streams range from -2.7 to -1.2, DG streams in our sample show only a 0.5 dex spread in mean metallicities. We then consider two different ways of comparing the DG streams to surviving dwarfs, assuming that present-day satellite galaxies are good proxies for progenitors of DG streams (Panithanpaisal et al. 2021). First, we compare the mean metallicities of the DG streams with known satellite galaxies of the MW (Simon 2019) and list galaxy analogs in Table 1. In particular, the progenitors of the Orphan-Chenab and Jhelum ($[Fe/H] \sim -1.8$) streams are expected to be similar to Leo II and Carina in luminosity $(M_V \sim -9.5)$, the progenitors of the Indus and Palca streams ([Fe/H] \sim -2.0) are expected to be similar to Draco and Sextans in luminosity ($M_V \sim -8.9$), and the progenitors of the Elqui and Turranburra streams ([Fe/H] ~ -2.2) are expected to be similar to Ursa Major I in luminosity $(M_V \sim -5)$. Second, we estimate the progenitor luminosities using the luminositymetallicity relation from Simon (2019), updated from Kirby et al. (2013b), shown on the upper axis of the right panel in

 $[\]overline{^{25}}$ Here we define the stream width, σ_w , as one standard deviation of a Gaussian profile. Some other analyses instead quote the FWHM = $2.355\sigma_w$.

Figure 2. Our DG streams' progenitors are at the faint end of the classical dSphs and the bright end of the UFDs.

Adopting the progenitor dynamical mass estimates based on stream widths from Shipp et al. (2018), the mass-to-light ratios of the progenitors of these DG streams are around 20–200 M_{\odot}/L_{\odot} , further supporting the conclusion that their progenitors are dark-matter-dominated DGs.

We compare the progenitor luminosities derived from metallicity with the present-day stellar mass of some streams presented in Shipp et al. (2018), assuming an $M_*/L_V=1.6$ (Kirby et al. 2013b). We find that the present-day stellar mass is lower than the progenitor mass. For example, the present-day stellar mass for the Elqui stream is about 50% of the estimated progenitor stellar mass, while for the Indus stream it is only $\sim 10\%$ of its estimated progenitor mass. This indicates that current photometric surveys are incomplete in their areal coverage of these streams (e.g., Chenab as part of the Orphan-Chenab stream) and/or in their achieved surface-brightness limit. Alternatively, it is possible that some stars in the stream are sufficiently phase mixed and thus difficult to detect above the background of the stellar halo (e.g., Johnston 1998; Helmi & White 1999).

3.3. Streams in Phase Space

With RVs from S⁵, PMs from Gaia EDR3, and distances derived in Section 2.3 for individual member stars, we now are able to study these streams in phase space. In this paper, we adopt the MW potential from the best-fit parameters of McMillan (2017), which include six components: bulge, dark matter halo, thin and thick stellar disks, and H I and molecular gas disks. We compute the following potential-dependent quantities for each stream member using gala v1.3 (Price-Whelan 2017; Price-Whelan et al. 2020) and galpot (Dehnen & Binney 1998): the total orbital energy E_{tot} , pericenter r_{peri} , apocenter $r_{\rm apo}$, eccentricity, and orbital period. We also compute potential-independent quantities: angular momenta L_Z and L_{XY} and orbital poles l_{pole} , b_{pole} . We take the Sun's position and 3D velocity from astropy (Astropy Collaboration et al. 2013, 2018) v4.0 with $d_{\odot} = 8.122 \,\mathrm{kpc}$ (Gravity Collaboration et al. 2018) and $v_{\odot} = (12.9, 245.6, 7.78) \text{ km s}^{-1}$ (Drimmel & Poggio 2018; Gravity Collaboration et al. 2018; Reid & Brunthaler 2004).

We present the phase-space distribution of the dozen streams in Figure 3. In the left panels, each symbol represents a single stream member star, with circles for GC stream members and crosses for DG stream members. In the right panels, we use an ellipse to show the 1σ contour assuming the distribution is a 2D Gaussian. From top to bottom, we show $E_{\rm tot}-L_{\rm Z}$, orbital poles, and peri/apocenters, respectively. Table 2 summarizes the orbital properties, which are computed as medians across member stars in each stream.

Two GC streams, 300S and Jet, have a positive L_Z and are therefore on retrograde orbits. Three streams—Ophiuchus, Jhelum, and Elqui—have a negative L_Z , and a much smaller $|L_Z|$ compared to L_{XY} ; hence we classify these three streams on near-polar orbits. The remaining seven streams are on prograde orbits. Except for Ophiuchus, all streams in our sample have Galactocentric distances larger than 10 kpc. All the streams

have pericenters less than 20 kpc, which is well matched with the fact that their progenitors were tidally disrupted.

We note that the large scatter in Figure 3 is mostly a result of measurement uncertainties, largely in the PM components. However, the large deviation between Orphan and Chenab is a result of the strong perturbation by the LMC (Erkal et al. 2019).

3.3.1. Association with MW Satellites

In order to study the possible associations between the streams and other MW satellite systems, we also compute the orbital properties of the MW's GCs and DGs as we did for the streams, using 6D information from Vasiliev & Baumgardt (2021) for GCs and A. B. Pace et al. (2022, in preparation) for DGs, treating each system as a single test particle. In order to compute the uncertainties of the orbits, for each DG or GC, we sample 1000 realizations from the reported uncertainties.

In Figure 3, we present the GCs that overlap with S^5 streams in orbital space. We first check their locations on the $E_{\rm tot}-L_Z$ plane, as we expect the energies and angular momenta of systems from the same progenitor or the same group infall to be similar in the absence of external perturbations. We then check the orbital poles and peri/apocenters to confirm the association. The orbital poles might be slightly off (by a few degrees) as they are expected to drift between multiple wraps (e.g., Erkal et al. 2016b). From this comparison, we find that three GCs (shown as open diamond symbols in the left panels of Figure 3) have possible connections with the dozen streams: NGC 5824 and Willka Yaku, NGC 5466, and 300S, and Laevens 3 and Orphan-Chenab. We summarize these findings in Table 2, with further discussion in Section 4.6.

For DGs, we limit our galaxy sample to those with median pericenter below 25 kpc and median apocenter below 90 kpc to better match the properties of the streams. These criteria result in a total of five UFDs: Segue 1, Segue 2, Willman 1, Draco II, and Tucana III, shown as open star symbols in the same figure. Due to the large uncertainties in the orbital properties (mainly coming from the distance and PM uncertainties of the DGs), many of the DGs overlap with streams in phase space within the 1σ uncertainties. For example, Willman 1's orbital energy, angular momentum, pericenter, and apocenter are all consistent with Willka Yaku, and Segue 1's orbital properties are similar to those of the Jet stream. Among these UFDs, only Tucana III has clear tidal tails present (Drlica-Wagner et al. 2015; Li et al. 2019), consistent with its extremely small pericenter (\sim 3 kpc). The other four UFDs have no clear detection of tidal tails, although some evidence of tidal effects has been reported (see, e.g., Kirby et al. 2013a). Given that these four DGs have pericenters similar to the other disrupted DG streams (i.e., $\lesssim 20$ kpc), further investigation might be needed to carefully examine these systems for possible tidal features. However, these DGs are all less luminous $(M_V > -3)$ and therefore are usually smaller in half-light radius than the progenitors of the DG streams in our sample, which may explain why these galaxies are more resistant to tidal disruption even though they lie on similar orbits to the DG streams. It is also worth mentioning that these five UFDs have ambiguous classifications between DGs and GCs except for Segue 1, for which both a clear velocity dispersion and metallicity dispersion have been identified (e.g., Norris et al. 2010; Simon et al. 2011).

 $[\]overline{^{26}}$ We adopt a right-handed coordinate system, in which a positive L_Z corresponds to a retrograde orbit.

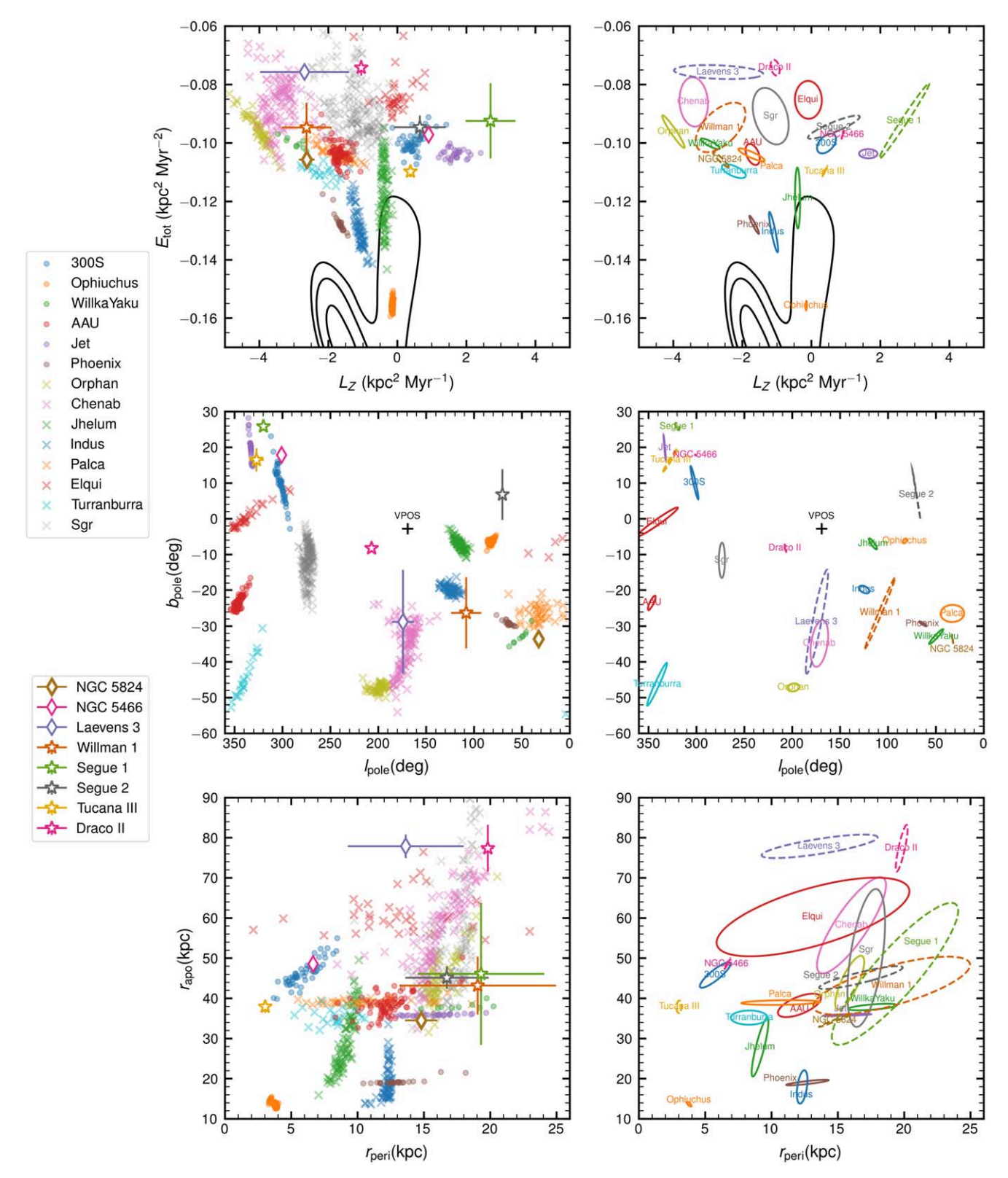


Figure 3. Orbital energy E_{tot} and angular momentum L_Z , where positive L_Z corresponds to a retrograde orbit (top row); orbital poles l_{pole} , b_{pole} , where positive b_{pole} corresponds to a retrograde orbit (middle row); and orbital pericenters and apocenters (bottom row), computed from the spectroscopic member stars of each stream. The left column shows the scatter plot for the full sample of individual stream members, with circles for GC streams and crosses for DG streams. To minimize crowding, only 10% of the Sgr stream members are shown. Also shown are GCs (DGs) that might be associated with streams, with diamond (star) symbols for the median values and error bars corresponding to one standard deviation. In the right column, ellipses with solid (dashed) lines present 1σ confidence levels for the streams (DGs or GCs). Note that some ellipses are very small. In the top row, the black contours show the density distribution of all S^5 stars, which is dominated by the disk (negative L_Z) and Gaia–Enceladus–Sausage (GES; $L_Z \sim 0$). In the middle row, the black plus sign shows the orbital pole of the "vast plane of satellites" (VPOS) from Pawlowski & Kroupa (2013).

 Table 2

 Orbital Properties of One Dozen Streams Observed with S^5

Stream	Orbit	$\frac{E_{\rm tot}}{({\rm kpc}^2/{\rm Myr}^2)}$	L_Z (kpc ² /Myr)	L_{XY} (kpc ² /Myr)	<i>l</i> _{pole} (°)	$b_{ m pole}$ (°)	r _{gal} ^a (kpc)	r _{peri} (kpc)	r _{apo} (kpc)	Eccentricity	Period (Myr)	Possible Association
300S	Retrograde	-0.10	0.44	2.65	302.0	10.1	22.2	5.8	45.8	0.77	560	NGC 5466
Ophiuchus	Polar	-0.16	-0.15	1.35	82.4	-6.2	4.3	3.8	13.7	0.57	180	
Willka Yaku	Prograde	-0.10	-2.93	4.63	49.7	-32.9	36.1	17.6	37.9	0.37	570	NGC 5824
AAU	Prograde	-0.10	-1.70	3.90	346.5	-23.5	26.1	12.1	38.2	0.51	520	Palca
Jet	Retrograde	-0.10	1.65	4.68	333.1	19.9	33.9	15.7	35.9	0.39	530	
Phoenix	Prograde	-0.13	-1.66	2.94	63.6	-29.3	18.9	12.7	19.1	0.20	320	
Orphan	Prograde	-0.10	-4.00	3.67	198.7	-47.1	17.6	15.9	43.9	0.47	630	
Chenab	Prograde	-0.09	-3.41	4.77	171.7	-34.8	28.0	16.0	58.2	0.56	800	Laevens 3
Jhelum	Polar	-0.12	-0.40	3.14	115.8	-7.0	10.8	9.1	27.8	0.51	380	
Indus	Prograde	-0.13	-1.10	3.04	124.8	-19.8	12.4	12.3	17.9	0.19	300	
Palca	Prograde	-0.10	-1.74	3.53	32.8	-26.5	38.5	10.7	39.0	0.57	520	Cetus, AAU
Elqui	Polar	-0.09	-0.09	5.18	339.0	-0.9	51.0	13.1	60.3	0.65	810	
Turranburra	Prograde	-0.11	-2.25	2.26	340.8	-46.3	31.7	8.3	35.2	0.62	460	

Note

4. Discussion

4.1. "Too Big to Fail" in Streams?

Cosmological simulations show that MW-mass dark matter halos have too many massive subhalos²⁷ compared to the MW's actual satellites, which is known as the "too big to fail" problem (Boylan-Kolchin et al. 2011, 2012). We find a possibly similar too big to fail problem with the number of massive stellar streams in simulations.

Using the FIRE-2 suite of cosmological simulations, Panithanpaisal et al. (2021) studied the stellar streams formed from disrupted satellite galaxies in a suite of MW-mass galaxies. These simulations resolve stellar streams with progenitor stellar masses between $5 \times 10^5 M_{\odot}$ and $10^9 M_{\odot}$, which are generally more massive than our DG stream progenitors. According to Figure 2, our most massive DG stream is Orphan-Chenab at $M_V \sim -9.1 \pm 1.4$, where the uncertainty comes from a scatter of 0.16 dex in [Fe/H] from the mass-metallicity relation (Simon 2019). This luminosity corresponds to $M_* \circ 6^{+15}_{-4} \times 10^5 M_{\odot}$, assuming $M_*/L_V = 1.6$ (Kirby et al. 2013b), which is at the lower-mass end of the streams in the FIRE-2 simulations. Except for the Sgr stream, none of the known MW DG streams have a stellar mass higher than the Orphan-Chenab stream²⁸ However, cosmological simulations from 13 MW-like galaxies predict a total of 3-10 streams in this mass range, with a median of 8, which is much higher than the number inferred from observations. If the stellar mass is not considered, the other way to interpret the observational result is that we have not found any DG streams with a mean metallicity between $[Fe/H] \sim -1.78$ (Orphan-Chenab) and $[Fe/H] \sim -0.5$ (Sgr). Two other DGs have shown possible tidal features, Antlia 2 and Crater 2; however, their metallicities are at [Fe/H] = -1.77 and [Fe/H] = -2.10, respectively (Ji et al. 2021). This is reminiscent of the "too big to fail" problem among MW satellites, and in fact, the two may share a common origin.

A few possibilities might alleviate this tension. First, it is possible that the simulations are overpredicting the number of massive streams, as the majority of these MW analogs $(M_{200} \sim 1.1 - 2.1 \times 10^{12} M_{\odot})$ are at the high end of the measured MW mass range, especially when the LMC is included in the fit. For example, Shipp et al. (2021) found that, when fitting the LMC mass with stellar streams, a lighter MW mass around $M \sim 0.8 \times 10^{12} \, M_{\odot}$ fits the stream data better. The smaller number of observed massive DG streams relative to simulations could therefore be a hint of a smaller value of the MW mass. Alternatively, more massive DG streams in the MW halo may yet be undiscovered, either at larger distances that cannot be reached with current survey depths or because the previous searches were biased toward metal-poor overdensity structures and missed the most metal-rich (and therefore massive) streams. Note that all DG streams presented in this paper were (partially) discovered in the DES data with a matched filter based on a metal-poor ($[Fe/H] \sim -1.9$), old (age = 13 Gyr) isochrone (Shipp et al. 2018).

4.2. Prograde versus Retrograde

Panithanpaisal et al. (2021) showed that from FIRE-2 simulations, we expect an even distribution of the satellite galaxies on prograde and retrograde orbits. However, as shown in Figure 3, the majority of our streams are on prograde orbits with $L_Z < 0$ (or $b_{\rm pole} < 0$). In particular, none of the DG streams are on retrograde orbits, except for Elqui, which is on a nearpolar, slightly retrograde orbit. Although these DG streams' progenitors are all less massive than those shown in Panithanpaisal et al. (2021), it is still striking that none of the DG streams from our sample are on a retrograde orbit. More intriguingly, as of now, none of the known DG streams in the MW are on retrograde orbits.

In Figure 4, we compare the orbital orientation of the streams to relatively luminous DGs in the MW with $M_V < -6$, as this luminosity threshold is similar to the faintest DG streams in our sample, as derived from their metallicities. Intriguingly, among these 16 DGs, only 2—Fornax and Crater 2—are on retrograde orbits, showing a strong imbalance in prograde versus retrograde orbits, similar to the streams. However, many of these are DGs clustered in the "vast plane of satellites" (VPOS)

^a Distance to the Galactic center, the median of all stream members.

More accurately, too many subhalos of high central density.

²⁸ Although GES, the Helmi Stream, and other newly discovered stellar substructures (e.g., Naidu et al. 2020) are likely from disrupted DGs, we do not consider them here as we only consider streams that are not phase mixed, following the same definition as used in Panithanpaisal et al. (2021).

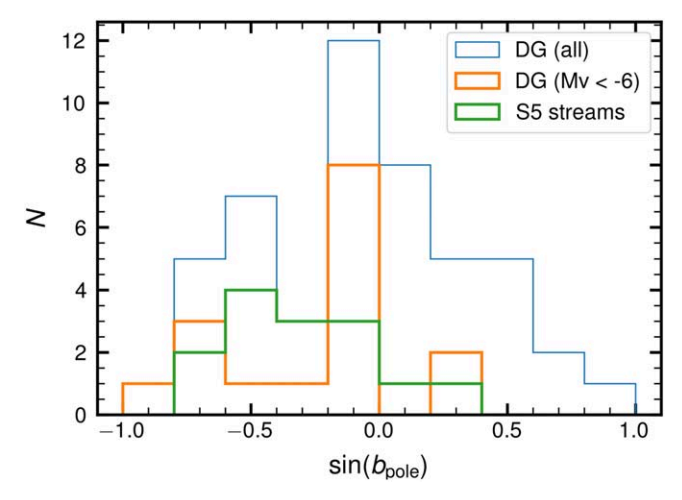


Figure 4. Distribution of $\sin(b_{\rm pole})$ for all MW DG satellites (blue), the brightest DG satellites (orange), and one dozen streams (green), where a positive (negative) $\sin(b_{\rm pole})$ corresponds to a retrograde (prograde) orbit. The distribution for all DG satellites is reasonably symmetric. The large spike at $\sin(b_{\rm pole}) \sim -0.1$ in the distribution of the brightest DG satellites corresponds to the VPOS plane satellites. Both the massive DG satellites and the dozen streams have a preference for prograde orbits.

(Pawlowski et al. 2012, 2015), the orbital pole of which is shown as the black "+" symbol in the top-right panel of Figure 3. Although both the streams and dSphs have a preference for prograde over retrograde orbits, the orbital poles of the streams do not seem to be clustered like the VPOS (Riley & Strigari 2020).

The preference for prograde orbits in both streams and relatively luminous DGs may suggest that dwarf galaxies, especially the most massive DGs, were accreted onto the MW via group infall from one filament at a time, resulting in strong clustering in either prograde or retrograde orbits. For example, the progenitors of some of these streams may have been accreted as a group early on with prograde orbits, while some of the relatively luminous DGs may have been accreted more recently from a single filament, resulting in a strong clustering in the VPOS plane.

4.3. Eccentricities and Orbital Phase

To study the orbital phase and eccentricity (e) of the dozen streams, we define the ratio f as a proxy to represent the orbital phase in the radial direction, $f = \frac{r_{\rm gal} - r_{\rm peri}}{r_{\rm apo} - r_{\rm peri}}$, which was first used by Fritz et al. (2018) to study the orbital phase of MW DGs; f = 0 indicates that the stream is close to the pericenter and f = 1 indicates that the stream is near apocenter. Here $r_{\rm gal}$ is the current distance to the Galactic Center. In the upper panel of Figure 5, we show the ratio f and eccentricity for every stream member. In the upper-right panel, we show the median value for each stream, where the circle and cross symbols show the median distance to the Galactic Center, and the arrows show the median pericenter and apocenter for each stream. Interestingly, among these dozen streams, four streams (Ophiuchus, Jhelum, Indus, and Orphan-Chenab) are close to pericenter, while six streams (Palca, Turranburra, Elqui, Jet, Willka Yaku, and Phoenix) are close to apocenter; only AAU and 300S have 0.2 < f < 0.8.

We include GCs and DGs in Figure 5 for comparison. For GCs, we only include those with Galactocentric distance $r_{\rm gal} > 10$ kpc to match our streams, which we refer to as distant

GCs in later discussion. In particular, we highlight those tidally filling (or "fluffy") GCs in red and compact GCs in blue (see details on the definitions in Baumgardt et al. 2010), many of which also display tidal features (Gieles et al. 2021). For DGs, we consider DGs whose apocenters are less than 300 kpc, which is close to the virial radius of the MW.

We also show the probability distribution (normalized to one) of the ratio f in the lower-left panel of Figure 5, for streams, DGs, and GCs, respectively. For GCs and DGs, each DG and GC is counted as one occurrence. For streams, we count each stream as one occurrence (here, Orphan and Chenab are considered one stream) but redistribute the weight to each stream member star evenly. Also plotted are the expected probabilities of f for an outer halo star in an orbit with an eccentricity of 0.2, 0.4, and 0.6, respectively, under the same McMillan (2017) MW potential. We compute the distribution by sampling stars with similar orbits to the streams, DGs and GCs, but at particular eccentricities. The sampled distributions present pileups near the pericenter and apocenter in f because $\frac{d}{dt}r_{\rm gal}$ is close to zero near pericenter and at apocenter. We see similar pileups in both pericenters and apocenters for the GCs and streams, indicating that there is no evidence for an observational selection effect reducing the observed number of streams or GCs near apocenter. On the other hand, DGs show similar pileups around pericenter but a deficiency near the apocenter of their orbits (e.g., Simon 2018; Fritz et al. 2018), indicating that a number of MW DG satellites near their apocenters may remain to be detected.

For the eccentricity, the upper panels show that the majority of streams are clustered around $e \sim 0.55$. In particular, except for the Indus stream, all DG streams have an eccentricity between 0.45 and 0.65. The eccentricity distribution of streams is most similar to the "fluffy" GCs, while compact GCs are more eccentric ($e \sim 0.9$) and nearby ($r_{\rm gal} < 40$ kpc), and DGs are less eccentric ($e \sim 0.4$) and more distant ($r_{\rm gal} > 40$ kpc), as shown in the upper-right panel of Figure 5.

4.4. Metallicity and Eccentricity of the GC streams

Figure 6 shows that four of the six GC streams have a mean metallicity [Fe/H] < -2, while a majority of the intact distant GCs have a mean metallicity > -2, indicating that the progenitors of our GC streams are in general more metal poor than the distant GCs. Such a difference in metallicity may point to a different origin for the GC streams compared to most of the distant GCs (e.g., accreted versus in situ formation). Alternatively, if both populations are accreted, the disrupted GC streams may have been accreted earlier, and therefore their progenitors could have been more metal poor. The latter possibility is also consistent with the fact that no clear progenitors are seen for any of the streams in our GC stream sample.

Even more interesting, we find that these six GC streams show a correlation between the mean metallicity and eccentricity of the stream, where more metal-rich streams are on orbits with higher eccentricity. As these streams' progenitors are likely GCs accreted together with their parent galaxies, the GC metallicity may be correlated with the metallicity (and thus the mass) of the parent galaxy. The GC metallicity distribution function (MDF) may not match the parent galaxy MDF exactly, but it is clear that high-metallicity GCs must come from more massive parent galaxies. Such a correlation could therefore be explained in two scenarios. The first

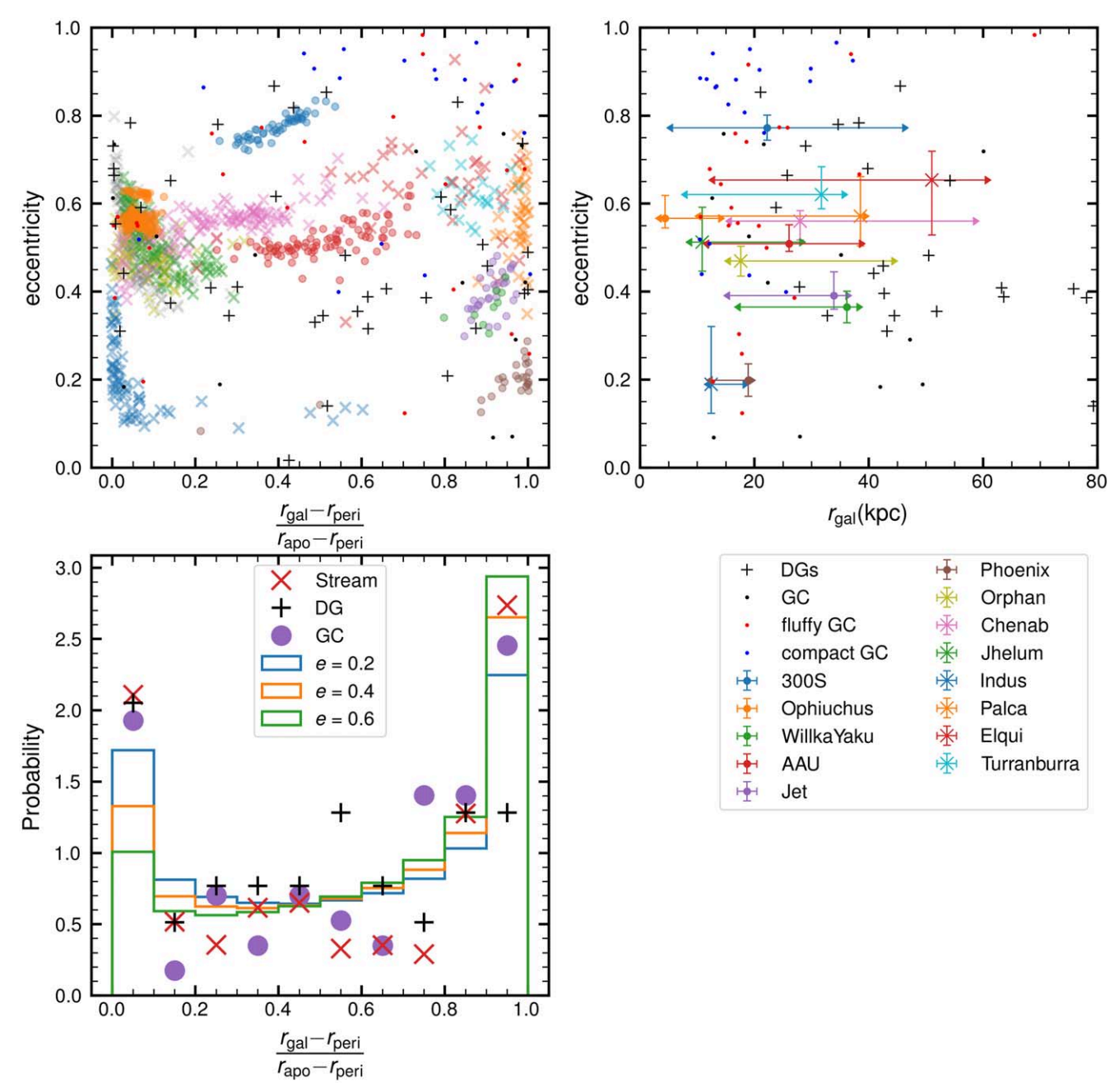


Figure 5. (Upper left) Eccentricity $e = \frac{r_{\rm apo} - r_{\rm peri}}{r_{\rm apo} + r_{\rm peri}}$ vs. ratio $f = \frac{r_{\rm gal} - r_{\rm peri}}{r_{\rm apo} - r_{\rm peri}}$. Each symbol corresponds to member stars in each stream. f = 0 (f = 1) indicates the star is close to the pericenter (apocenter). Also plotted are GCs (black dots) and DGs (black plus symbol). Only GCs with Galactocentric distances larger than 10 kpc are shown; only DGs with apocenters smaller than 300 kpc are shown. In addition, we highlight those "fluffy" GCs in red and "compact" GCs in blue, defined in Baumgardt et al. (2010) and Gieles et al. (2021). (Upper right) eccentricity vs. Galactocentric distance to the streams ($r_{\rm gal}$), where the circles and cross symbols indicate the current location of the stream and triangles show the pericenter and apocenter of each stream. Each symbol corresponds to one stream, calculated as the median value of all stream members shown on the upper left. The error bars on the eccentricities show the 16th and 84th percentiles from all stream members. (Lower left) Histogram of the ratio f for the stream, DG, and GC, respectively. Also plotted are the expected distributions for an outer halo star in an orbit with an eccentricity of 0.2, 0.4, and 0.6, respectively, under the same MW potential. The distributions predict a pileup near $f \sim 0$ and $f \sim 1$, which matches what is seen in the GCs and streams. However, the current known DGs have a lack of pileup at apocenter relative to predictions.

explanation is that the larger-eccentricity GC streams are usually associated with a massive (and therefore more metalrich) and recent merger, while the low-eccentricity GC streams are accreted earlier with relatively metal-poor galaxies. Recent simulations also show a trend between the accretion time and eccentricity, where high0eccentricity stars are likely associated with a recent merger event (Mackereth et al. 2019). Alternatively, assuming all these GCs' parent galaxies were accreted at a similar time, then as a result of dynamical friction,

the orbits of the more-massive galaxies tend to become more radial and eccentric faster than those of lower-mass galaxies (although the details depend on other factors like the initial orbital eccentricity; Vasiliev et al. 2022).

We also show the eccentricity and metallicity of distant GCs in the same panel. Most of these distant GCs have a higher metallicity and also a higher eccentricity and show a weaker metallicity–eccentricity correlation than our GC streams.

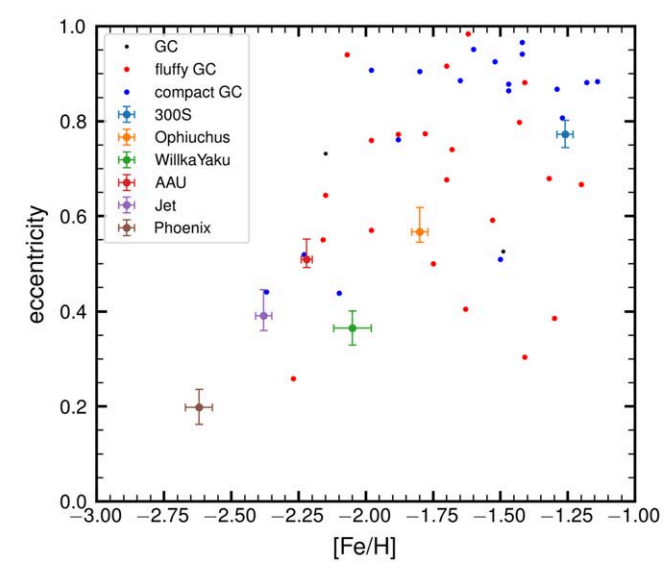


Figure 6. Eccentricity vs. mean metallicity for all GC streams, showing a trend that more metal-rich streams are on higher-eccentricity orbits. Also shown are known GCs whose Galactocentric distances are larger than 10 kpc. Metallicities of GCs are taken from Harris (2010). The GC streams have, in general, lower metallicities than GCs at similar distances.

We note that such a relation in the streams could just be a coincidence due to the small sample size. The relation is largely driven by the two most extreme streams. 300S, the most metalrich stream in our sample, is possibly associated with a very radial merger, GES, which was likely accreted ~10 Gyr ago (e.g., Belokurov et al. 2018; Helmi et al. 2018; Naidu et al. 2021). On the other hand, the Phoenix stream has a metallicity lower than any known GC (Wan et al. 2020) and also seems to have a more circular orbit than any known distant GC. As the dissolution time of a GC stream is anticorrelated with the eccentricity (Baumgardt & Makino 2003), Phoenix's progenitor would have a maximum lifetime possible in its orbit. This may explain why it is not fully mixed yet, even though it might have fallen into the MW a long time ago, given its extremely low metallicity.

Finally, we note that we do not see such a correlation in our DG streams because the metallicity range for DG streams is very narrow, as shown in the right panel of Figure 2.

4.5. Stream Velocity Dispersions

DG streams are expected to have larger velocity dispersions than GC streams (Figure 2) due to the large dynamical mass of their progenitors' dark matter halos. However, Elqui, Jhelum, Palca, and Turranburra show dispersions that are larger than 13 km s⁻¹, which is higher than every MW satellite galaxy (Simon 2019) except for the LMC and Small Magellanic Cloud (SMC). Because the inferred stellar masses of the progenitors of DG streams are smaller than most of the classical dSph satellites, and conservation of phase-space density would suggest that velocity dispersion of a stream should decrease with time (Helmi & White 1999), the extremely large velocity dispersion suggests that additional processes have heated the streams. Interestingly, except for Jhelum—whose large velocity dispersion may be associated with its complicated morphology (Bonaca et al. 2019; Shipp et al. 2019)—the other three streams with large velocity dispersions are all near apocenter, as shown in the left panel of Figure 7. This suggests the dispersion of DG

streams might be correlated with the stream's orbital phase. However, Panithanpaisal et al. (2021) found in the FIRE-2 simulations that streams near pericenter tend to have higher velocity dispersions, contrary to what is shown in Figure 7.

We also explore the relation between velocity dispersion and pericenter, shown in the right panel of Figure 7. The four DG streams with large velocity dispersions have relatively small pericenters compared to the Orphan-Chenab stream, which has the lowest velocity dispersion among all DG streams. In contrast, although the Indus stream has a small pericenter, its eccentricity is also much smaller than that of the other five DG streams. The large velocity dispersions observed for some DG streams may be explained by a combination of the eccentricity and pericenter of each stream. For GC streams, such a relation would be expected because the streams with small pericenters and large eccentricities will have correspondingly smaller tidal radii (Küpper et al. 2012) and thus larger velocity dispersions for the stripped stars. However, for the observed dwarf galaxies, the velocity dispersion does not strongly depend on the radius (e.g., Walker et al. 2007). Thus, more theoretical work is needed to determine if this could explain the entirety of the effect.

Alternatively, Errani et al. (2015) argued that the internal dynamics of tidal streams are largely affected by the dark matter profile in which their progenitors are embedded; a larger velocity dispersion in the DG streams may indicate that the progenitors were embedded in a cored dark matter halo instead of a cuspy one. Our DG stream sample would be a valuable sample for such cusp/core dark matter profile studies.

On a similar note but different from the DG streams, Malhan et al. (2021a) proposed that the dynamical properties of accreted GC streams are also sensitive to the central dark matter density profile of their parent DGs—GC streams are dynamically hotter if their parent DGs reside in a cuspy subhalo than if they reside in a cored subhalo. In their simulations, GC streams originating from a cuspy parent subhalo have velocity dispersions larger than 4 km s⁻¹. All our GC streams have velocity dispersions below 4 km s⁻¹, suggesting that if the modeling from Malhan et al. (2021b) is correct and our GC streams are indeed accreted, the progenitors of these GC streams resided in cored subhalos.

Finally, we note that our inferred velocity dispersions could be inflated by nonmembers or binary star motions. This is especially relevant for the dwarf galaxy streams, as the intrinsic metallicity spread makes it harder to remove foreground stars.

4.6. Stream Associations with Other Objects

Dwarf galaxies can accrete with a population of their own globular clusters or dwarf galaxy satellites. We thus might expect to see kinematic associations between our streams and/or other halo objects. Conversely, it should be possible to associate GC streams with their parent dwarf galaxies, whether those galaxies are intact or tidally disrupted. We now discuss several likely associations.

4.6.1. 300S, NGC5466, Tucana III and Gaia-Enceladus-Sausage

Fu et al. (2018) argued that the 300S progenitor was likely to be a compact DG, based on the chemical abundances of 300S member stars from APOGEE and SEGUE. We do not detect a metallicity dispersion with a much larger sample of 300S member stars, and 300S has a small stream width of $\sigma_w = 0.4^{\circ}$

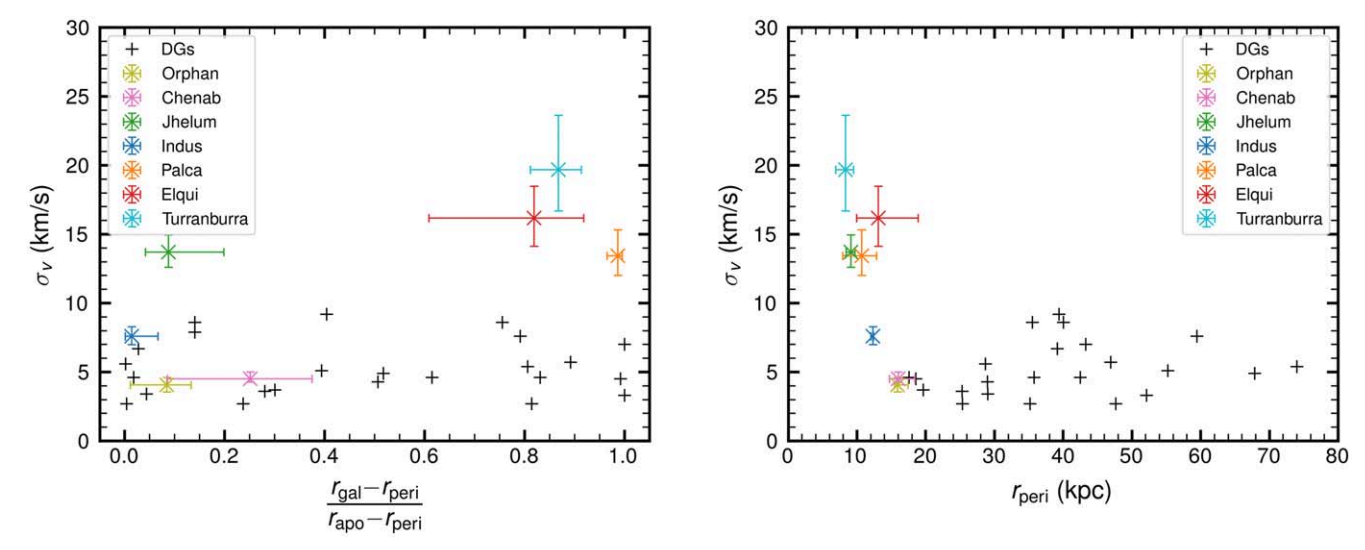


Figure 7. (Left) Velocity dispersion of DG streams vs. ratio $f = \frac{r_{\rm gal} - r_{\rm peri}}{r_{\rm apo} - r_{\rm peri}}$. The error bars are computed from the 16th and 84th percentiles of all stream members. Except for Jhelum, streams with large velocity dispersions are located near the apocenters of their orbits. (Right) Velocity dispersion of DG streams versus their pericenters. Streams with the smallest pericenters tend to have larger velocity dispersions. For both panels, MW DG satellites with a resolved velocity dispersion are also shown, which mostly have velocity dispersions <10 km s⁻¹. We note that in the right panel, there appears to be a deficiency of DGs with $r_{\rm peri}$ < 20 kpc. Actually, a few DGs or DG candidates—such as Tucana III, Segue 2, Draco II, and Triangulum II—have pericenters less than 20 kpc. However, as these systems only have upper limits for their velocity dispersions, they are not included in this plot.

or ~110 pc (at a heliocentric distance of 16 kpc), similar to other GC streams.²⁹ Thus, we argue that 300S's progenitor is more likely to be a GC than a DG. Furthermore, given its high metallicity ([Fe/H] ~ -1.3), if it is a DG, then it would have been very massive, according to the galaxy mass-metallicity relation. This is unlikely unless the progenitor is the compact core or the nucleated star cluster of a massive galaxy. Given its location on the $E_{\text{tot}}-L_Z$ plane in Figure 3 and its high eccentricity (e = 0.80) and metallicity, we postulate that 300S's progenitor was highly likely to have been a GC of a past merger on a polar-to-retrograde orbit, very likely to be GES (Belokurov et al. 2018; Helmi et al. 2018). Alternatively, 300S's progenitor may be the nucleated star cluster of GES; this picture might also match with the abundance pattern seen in Fu et al. (2019) from APOGEE. More high-resolution spectroscopic observations on 300S might solve this puzzle.

NGC 5466 overlaps with 300S in the $E_{\text{tot}}-L_Z$ plane and has almost identical orbital poles and peri/apocenters to 300S. However, the metallicity of NGC 5466 ([Fe/ H] = -1.97 ± 0.13 ; Lamb et al. 2015) is significantly more metal poor than that of 300S ([Fe/H] ~ -1.3), making it unlikely to be the direct progenitor of 300S. Similarly, Tucana III is also very close to 300S in the E_{tot} - L_Z plane with a high eccentricity, but its mean metallicity ([Fe/H] ~ -2.5 ; Simon et al. 2017; Li et al. 2019) is also much lower. Both NGC 5466 and Tucana III show tidal tail features (Belokurov et al. 2006; Drlica-Wagner et al. 2015), although the progenitor cores are not yet fully disrupted. It is possible that NGC 5466, Tucana III, and the progenitor of 300S are satellite GCs or UFDs from the same infall of their potential parent galaxy, GES.

4.6.2. Palca, Cetus, and AAU

Although the Palca stream was discovered in DES (Shipp et al. 2018), no specific observations were planned by S^5 (Li

et al. 2019) due to its extremely diffuse structure. However, Li et al. (2021) detected a second structure with a heliocentric velocity of $\sim\!100~{\rm km\,s^{-1}}$ in the AAU field. Based on its location, PM, and heliocentric distance, Li et al. (2021) argued this kinematically cold structure is associated with the Palca stream. Chang et al. (2020) argued that Palca is likely the southern extension of the Cetus stream. Our Palca stream data match the kinematic prediction of Chang et al. (2020), confirming that Cetus and Palca are indeed one stream. A more detailed study of this connection is discussed in Yuan et al. (2021).

Although Palca member stars are identified in the AAU field, the PMs of the Palca members are almost perpendicular to those of the AAU stars. Their RVs also differ by >100 km s⁻¹. Therefore, no connections were originally considered between these two streams. Instead, Li et al. (2021) pointed out that AAU's orbit is very close to that of Whiting 1, NGC 5824, and Pal 12 in action space, which are themselves possibly associated with the Sgr dwarf according to Massari et al. (2019). Li et al. (2021) therefore suggested that the progenitor of the AAU stream might have been accreted with the Sgr dwarf.

Interestingly, we find here that the AAU stars and Palca stars exactly overlap in the $E_{\rm tot}-L_Z$ plane (upper panels of Figure 3) and show very similar peri/apocenters (lower panels of Figure 3). The orbital poles of the two streams are also very close (middle panels) but are slightly different in longitude ($l_{\rm pole}$), which is expected between multiple wraps in a nonspherical potential. We therefore argue that AAU is more likely to be associated with the Palca/Cetus stream than with the Sgr stream and is likely on a different wrap from Palca, which leads to a small drift in the orbital pole. Because the metallicity mean and dispersion of the two streams are slightly different, it is unlikely that the two streams share the same progenitor. However, it may be that AAU's progenitor was a GC of Palca's progenitor. This possibility would be exciting because no GCs have been found around DGs at similar

 $[\]overline{^{29}}$ $\sigma_w = 0.4^\circ$ corresponds to an FWHM stream width of 0°94 reported in Fu et al. (2018).

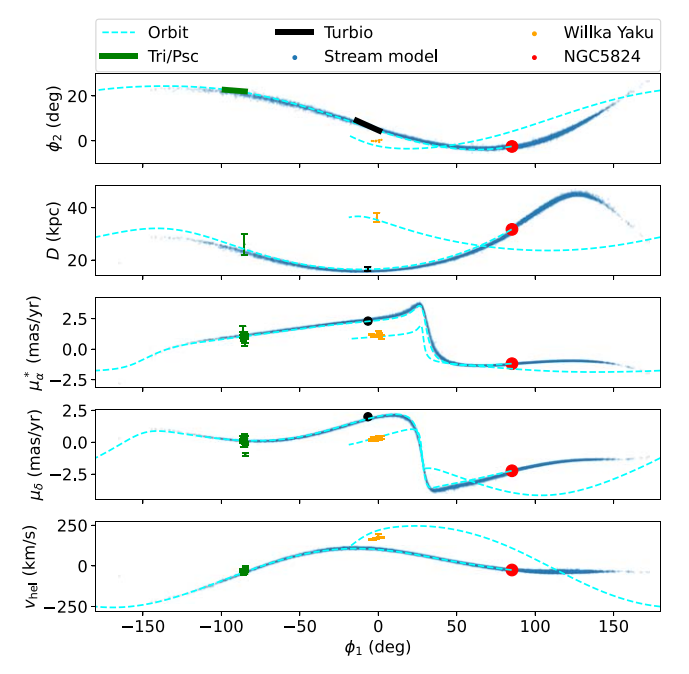


Figure 8. Comparison between the stream model of NGC 5824, the orbit of NGC 5824, and the Turbio, Triangulum/Pisces, and Willka Yaku streams. The blue particles show the predicted stream of NGC 5824, and the dashed cyan line shows the future orbit of NGC 5824. The red circle shows the location of NGC 5824. The green, black, and yellow symbols show the observables of Tri/Psc, Turbio, and Willka Yaku, respectively. The coordinate systems ϕ_1 and ϕ_2 are defined in Willka Yaku stream coordinates, using the transformations defined in Shipp et al. (2019).

metallicities to Palca ([Fe/H] = -2.0; e.g., Draco, Sextans, etc.).

We also note that several studies have suggested that NGC 5824 might be associated with the Cetus (i.e., Palca) stream (e.g., Newberg et al. 2009; Yuan et al. 2019). Bonaca et al. (2021) also suggested that Willka Yaku might be related to the Cetus stream. Indeed Figure 3 shows that Palca/Cetus, AAU, NGC 5824, and Willka Yaku are all very close in phase space and are likely all from the same group infall. However, based on the $E_{\rm tot}-L_Z$ and poles, we conclude that Palca and AAU are more closely connected, and Willka Yaku and NGC 5824 are more closely connected (see next section).

4.6.3. NGC 5824, Willka Yaku, Turbio, and Triangulum/Pisces

As shown in Figure 3, Willka Yaku and NGC 5824 have very similar energies, angular momenta, and orbital poles, suggesting they may have a common origin. Kuzma et al. (2018) found that NGC 5824 is remarkably extended in size, which might be an indication of tidal stripping. Bonaca et al. (2021) argued that NGC 5824 may be the progenitor of both the Triangulum and Turbio streams. We therefore study the connections between these three streams and NGC 5824, shown in Figure 8.

The Triangulum stream was first discovered by Bonaca et al. (2012) in photometric data from the Sloan Digital Sky Survey Data Release 8 (SDSS DR8) at a distance of $26\pm4\,\mathrm{kpc}$. Shortly thereafter, Martin et al. (2013) found a kinematically cold structure in a similar part of the sky with spectroscopic

data from SDSS DR8, which they dubbed the Pisces Stellar Stream. Here we refer to this structure as the Triangulum/ Pisces (or Tri/Psc) stream. In Figure 8, we show the on-sky position and distance from Bonaca et al. (2012),³⁰ and the PMs and RVs of likely members found by Martin et al. (2013), cross-matched with Gaia EDR3 and SDSS. Observations of Turbio are planned but have not yet been conducted by S^5 ; we therefore show the on-sky position and distance from Shipp et al. (2018) and proper motion from Shipp et al. (2019).

In order to explore the predicted debris of the NGC 5824 globular cluster, we use the modified Lagrange Cloud stripping method (Gibbons et al. 2014) as implemented in Erkal et al. (2019) to include the effect of the LMC. For the MW potential, we use a realization drawn from the posterior chains in McMillan (2017), for which Shipp et al. (2021) gave a good match to seven MW streams (see Table A3 of Shipp et al. 2021 for the potential parameters). We model the LMC as a Hernquist profile (Hernquist 1990) with a mass of 1.5×10^{11} and a scale radius of 17.13 kpc, which matches the rotation curve measurements of the LMC at 8.9 kpc (van der Marel & Kallivayalil 2014). For the present-day position and velocity of the LMC, we use measurements of its PM (Kallivayalil et al. 2013), distance (Pietrzyński et al. 2013), and RV (van der Marel et al. 2002). We model the progenitor of NGC 5824 as a Plummer sphere matching the observed mass and half-light radius (Baumgardt & Hilker 2018).

The blue dots in Figure 8 show the stream model of NGC 5824 (position and velocity taken from Vasiliev & Baumgardt 2021) stripped for 6 Gyr. The stream particles match those from Turbio and Tri/Psc perfectly but do not go through Willka Yaku. We note that if the LMC is ignored, the agreement of the NGC 5824 stream with Tri/Psc and Turbio is worse. Next, we consider whether Willka Yaku is consistent with a past or future orbit of NGC 5824 including the LMC. This is done by rewinding NGC 5824 for 6 Gyr in the presence of the MW and LMC. At this time, the LMC is far from the MW (\sim 425 kpc in the models used here), and the inner regions of the MW can approximately be thought of as isolated. Particles are then placed along this past orbit (between 4–6 Gyr ago with a spacing of 0.5 Myr), initialized at the same time of 5 Gyr in the past, and integrated to the present. If there were no LMC, these particles would lie along the orbit of NGC 5824, but with the LMC, these particles will instead represent the original orbit of NGC 5824 before the LMC's infall. The blue dashed line shows the leading orbit of NGC 5824 using this technique. Member stars in Willka Yaku are closer to the orbit of NGC 5824 in a second wrap but still have a small offset in the on-sky position and RV. We therefore conclude that, while NGC 5824 is likely the progenitor of Turbio and Tri/Psc, it is less likely the progenitor of Willka Yaku. However, given how similar their orbits are, it is very likely that the progenitors of Willka Yaku and NGC 5824 fell into the MW together.

Although Willka Yaku sits close to the future orbit of NGC 5824, the stream model does not reach its location despite being disrupted for 6 Gyr. Interestingly, Willka Yaku appears to sit at a lower energy than NGC 5824 (see Figure 3), which is inconsistent with it being in the leading debris of NGC 5824. However, there are significant uncertainties in this energy, and the energy may also have changed significantly due to

 $[\]frac{30}{30}$ Note that Martin et al. (2013) found the distance of the Pisces stream to be 35 ± 3 kpc. We did not use this distance because the distance from Bonaca et al. (2012) is a better fit to our model.

perturbations since they were accreted, e.g., by Sgr, the LMC, or other galaxies.

The metallicities for these systems are also very similar. NGC 5824's metallicity is $[Fe/H] = -1.94 \pm 0.10$ (Roederer et al. 2016). We find Willka Yaku's metallicity to be $[Fe/H] = -2.05 \pm 0.07$. Martin et al. (2013) reported a spectroscopic metallicity of [Fe/H] = -2.2 for Tri/Psc.

Roederer et al. (2016) found that NGC 5824 showed internal heavy element abundance variations. It will therefore be interesting to search for similar abundance patterns in Willka Yaku, Turbio, and Tri/Psc with high-resolution spectroscopy.

4.6.4. Indus, Jhelum, and LMS-1

Bonaca et al. (2019) suggested that Jhelum and Indus are tidal debris from the same DG at different orbital phases based on their 3D orbits. Our calculations show that the orbital properties of these two streams are close but quite distinct. Furthermore, their mean metallicities differ by more than 1.5σ . We therefore conclude that the two streams are unlikely to share the same progenitor, unless the progenitor possessed a significant metallicity gradient, causing a metallicity variation along the stream.

Malhan et al. (2021b) argued that the LMS-1 stream (Yuan et al. 2020) may be associated with the Indus stream based on their orbital properties. Our metallicity measurements for Indus ([Fe/H] \sim –2.0) are similar to those for the LMS-1 stream ([Fe/H] \sim –2.1), but Indus shows a significantly smaller velocity dispersion (\sim 7.5 km s $^{-1}$ for Indus and \sim 20 km s $^{-1}$ for LMS-1 from Malhan et al. 2021b). This is consistent with the suggestion of Malhan et al. (2021b) that the progenitor of Indus was a satellite galaxy of the progenitor of LMS-1.

4.6.5. Orphan-Chenab and Laevens 3

The Laevens 3 GC (Laevens et al. 2015) overlaps with the Chenab stream in phase space. Longeard et al. (2019) found a mean metallicity of $[Fe/H] = -1.8 \pm 0.1$ for Laevens 3, which is consistent with Orphan-Chenab's metallicity. We therefore tentatively suggest that Laevens 3 is likely a GC that was accreted along with the Orphan-Chenab stream's DG progenitor. However, due to the potential influence of the LMC, more sophisticated modeling is necessary to confirm this association. We leave this detailed study to S. E. Koposov et al. (2022, in preparation).

4.6.6. Clusters in the Smallest Galaxies

Among the MW satellites, the LMC, SMC, Fornax, and the Sgr dSph are known to have their own GCs. However, lower-mass DGs such as Sculptor, Carina, Sextans, and Draco have no GCs. With the exception of the Eridanus II DG at \sim 380 kpc (Bechtol et al. 2015; Koposov et al. 2015), none of the galaxies with luminosities below that of Fornax ($M_V \sim -13.5$) are known to host GCs. However, in this work, we found several possible associations that suggest that some Draco-to-Carinalike galaxies may have possessed GCs, including AAU's progenitor in Palca and Laevens 3 in Orphan-Chenab. If any of these associations are real, they would move the boundary for the formation of GCs in the DGs to lower luminosities (e.g., Kruijssen 2020; Wan et al. 2020) and may also affect our understanding of the specific frequency of GCs in DGs (e.g., Huang & Koposov 2021).

5. Conclusions

We report the orbital and chemical properties of 12 stellar streams that have a robust detection of spectroscopic members in the current S^5 data set. Three other streams were observed by S^5 with no clear spectroscopic member detection. None of these streams have a clear progenitor embedded in the stream. Using line-of-sight velocities from S^5 , PMs from Gaia EDR3, and distances derived from BHB and RRL tracers, we summarize the properties of the streams in Tables 1 and 2 and draw the following conclusions for these streams:

- 1. The velocity dispersions and metallicity dispersions show that half of these streams have DG progenitors, while the other half originates from disrupted GCs (Figure 2).
- 2. Our stream sample shows a significantly higher percentage of streams on prograde orbits than on retrograde orbits (Figures 3 and 4). Out of the dozen streams, seven are on prograde orbits, three are on polar orbits, and the remaining two streams are on retrograde orbits. The most-luminous DGs in the MW show a similar bias toward prograde orbits; only 2 out of the 16 most-luminous MW satellites are on retrograde orbits. The fact that both massive DGs and our stream sample show a preference for prograde orbits may suggest that groups of massive galaxies have been accreted onto the MW through group infall, resulting in a nonuniform distribution of the orbital poles (Section 4.2).
- 3. For streams from disrupted DGs, the mean metallicities range from [Fe/H] = -2.2 to -1.8. The corresponding luminosities of the progenitors range from $M_V \sim -6$ to $M_V \sim -10$, using the mass-metallicity relation from Kirby et al. (2013b). The fact that none of these DG streams are in a similar mass range to those in the FIRE-2 simulation may indicate that the "the too big to fail" problem observed in MW satellite galaxies extends to stellar streams (Section 4.1).
- 4. For streams from disrupted GCs, the mean metallicities have a much wider range, from [Fe/H] = -2.7 to -1.2. Our GC streams are in general more metal poor than MW GCs at similar distances (Figure 6), suggesting that either the progenitors of the GC streams have a different origin or a different accretion history from the distant MW GCs that are not yet fully disrupted. We also find a clear trend from six GC streams that more metal-rich streams lie on more eccentric orbits (Section 4.4).
- more eccentric orbits (Section 4.4).

 5. We compute the ratio $f = \frac{r_{\rm gal} r_{\rm peri}}{r_{\rm apo} r_{\rm peri}}$ as an analog of the orbital phase of the streams in the radial direction and find that 50% of the streams are near apocenter and 30% of the streams are near pericenter, matching expectations of apocenter and pericenter pileup (Figure 5). We compare with GCs and DGs in the MW and find that although the pileup at pericenter for DGs matches with the streams and GCs as well as expectation, there is a clear lack of DGs at apocenter. In addition, the eccentricities of the streams are mostly similar to those of the fluffy GCs in the MW, higher than the DGs, and lower than the compact GCs at similar distances (Figure 5 and Section 4.3).
- 6. Four DG streams show large velocity dispersions ($\gtrsim 10$ km s⁻¹), which may result from a combination of high eccentricity and small pericenter of the stream orbits

(Section 4.5). On the other hand, all our GC streams show a velocity dispersion below 4 km s^{-1} .

7. We compare the orbital properties of the streams to those of DGs and GCs in the MW, finding several possible associations (Section 4.6). In particular, the AAU stream's progenitor might be a GC of the Palca stream; NGC 5824 and the progenitor of the Willka Yaku stream may have fallen into the MW together; Laevens 3 might be a GC of the Orphan-Chenab stream; and NGC 5466, Tucana III, and the progenitor of 300S may have fallen into the MW together with a massive merger, likely GES. We emphasize that these associations are based on the locations of these substructures in the $E_{tot}-L_Z$ plane (Figure 3). Further modeling work and/or observations are necessary to confirm these connections. Finding GCs or GC streams that are associated with DG streams will inform our understanding of the formation of GCs in the smallest galaxies.

This paper mainly focuses on the properties of the dozen streams observed in S^5 as our first results, serving as a starting point to understand the distant (\gtrsim 10 kpc) stream population in the MW halo. Recently, many other streams (e.g., Ibata et al. 2019, 2021) and substructures (e.g., Naidu et al. 2020) have been discovered with Gaia and other spectroscopic efforts. We defer a more thorough discussion of these connections to a future paper.

In addition to the study of stream properties presented in this work, this stream sample is also a unique data set that may be used to study small-scale perturbations. In particular, 300S and Jet are both GC streams on retrograde orbits and are therefore ideal targets for stream density variation modeling in order to search for evidence of dark matter subhalo flybys. Furthermore, these dozen streams would also be an ideal sample to constrain the MW potential to high precision (Bonaca & Hogg 2018). However, we note that many of these streams are strongly affected by the LMC, which will be essential to model in such fits (e.g., Erkal et al. 2019; Shipp et al. 2021).

 S^5 has announced its first public data release (DR1; Li & S5 Collaboration 2021)³¹, which contains all targets observed in 2018–2019 following the target selection, data reduction, and survey validation described in Li et al. (2019). The following streams mentioned in this paper are included in DR1: AAU, Elqui, Indus, Jhelum, Orphan, Chenab, Palca, Phoenix, Willka Yaku, Sgr, and Ravi (no detection). Observations taken in 2020–2021 are expected to be released in S^5 DR2 in late 2022.

The authors would like to thank the referee for detailed comments that helped clarify the paper. T.S.L. would like to thank Ray Carlberg, Rohan Naidu, Ted Mackereth, Zhen Yuan, Nondh Panithanpaisal, and Robyn Sanderson for helpful discussion. T.S.L. also would like to thank Jiang Chang for sharing his Cetus model for comparison with our Palca data. T. S.L. is supported by NASA through Hubble Fellowship grant HST-HF2-51439.001 awarded by the Space Telescope Science Institute, which is operated by the Association of Universities for Research in Astronomy, Inc., for NASA, under contract NAS5-26555. A.B.P. is supported by NSF grant AST-1813881. S.L.M., J.D.S., and D.B.Z. acknowledge the support of the Australian Research Council through Discovery Project

grant DP180101791, and this research has also been supported in part by the Australian Research Council Centre of Excellence for All Sky Astrophysics in 3 Dimensions (ASTRO 3D), through project number CE170100013. S.L.M. and J.D.S. are supported by the UNSW Scientia Fellowship program. EB acknowledges support from a Vici grant from the Netherlands Organization for Scientific Research (NWO). A.P.J. acknowledges a Carnegie Fellowship and support from the Thacher Research Award in Astronomy.

This paper includes data obtained with the Anglo-Australian Telescope in Australia. We acknowledge the traditional owners of the land on which the AAT stands, the Gamilaraay people, and pay our respects to elders past and present.

This research has made use of the SIMBAD database, operated at CDS, Strasbourg, France (Wenger et al. 2000). This research has made use of NASA's Astrophysics Data System Bibliographic Services.

This paper made use of the Whole Sky Database (wsdb) created by Sergey Koposov and maintained at the Institute of Astronomy, Cambridge by Sergey Koposov, Vasily Belokurov, and Wyn Evans with financial support from the Science & Technology Facilities Council (STFC) and the European Research Council (ERC).

This work has made use of data from the European Space Agency (ESA) mission Gaia (https://www.cosmos.esa.int/gaia), processed by the Gaia Data Processing and Analysis Consortium (DPAC, https://www.cosmos.esa.int/web/gaia/dpac/consortium). Funding for the DPAC has been provided by national institutions, in particular the institutions participating in the Gaia Multilateral Agreement.

This project used public archival data from the Dark Energy Survey (DES). Funding for the DES Projects has been provided by the US Department of Energy, the US National Science Foundation, the Ministry of Science and Education of Spain, the Science and Technology Facilities Council of the United Kingdom, the Higher Education Funding Council for England, the National Center for Supercomputing Applications at the University of Illinois at Urbana-Champaign, the Kavli Institute of Cosmological Physics at the University of Chicago, the Center for Cosmology and Astro-Particle Physics at the Ohio State University, the Mitchell Institute for Fundamental Physics and Astronomy at Texas A&M University, Financiadora de Estudos e Projetos, Fundação Carlos Chagas Filho de Amparo à Pesquisa do Estado do Rio de Janeiro, Conselho Nacional de Desenvolvimento Científico e Tecnológico and the Ministério da Ciência, Tecnologia e Inovação, the Deutsche Forschungsgemeinschaft, and the Collaborating Institutions in the Dark Energy Survey. The Collaborating Institutions are Argonne National Laboratory, the University of California at Santa Cruz, the University of Cambridge, Centro de Investigaciones Energéticas, Medioambientales y Tecnológicas-Madrid, the University of Chicago, University College London, the DES-Brazil Consortium, the University of Edinburgh, the Eidgenössische Technische Hochschule (ETH) Zürich, Fermi National Accelerator Laboratory, the University of Illinois at Urbana-Champaign, the Institut de Ciències de l'Espai (IEEC/CSIC), the Institut de Física d'Altes Energies, Lawrence Berkeley National Laboratory, the Ludwig-Maximilians Universität München and the associated Excellence Cluster Universe, the University of Michigan, the National Optical Astronomy Observatory, the University of Nottingham, The Ohio State University, the OzDES Membership Consortium, the

³¹ DR1 is based on iDR1.5 and is now available at https://zenodo.org/record/4695135.

University of Pennsylvania, the University of Portsmouth, SLAC National Accelerator Laboratory, Stanford University, the University of Sussex, and Texas A&M University. Based in part on observations at Cerro Tololo Inter-American Observatory, National Optical Astronomy Observatory, which is operated by the Association of Universities for Research in Astronomy (AURA) under a cooperative agreement with the National Science Foundation.

Facility: Anglo-Australian Telescope (AAOmega+2dF). Software: numpy (van der Walt et al. 2011), scipy (Jones et al. 2001), matplotlib (Hunter 2007), seaborn (Waskom et al. 2016), astropy (Astropy Collaboration et al. 2013, 2018), RVSpecFit (Koposov 2019) q3c (Koposov & Bartunov 2006), emcee (Foreman-Mackey et al. 2013), gala (Price-Whelan 2017; Price-Whelan et al. 2020), galpot (Dehnen & Binney 1998).

ORCID iDs

```
Ting S. Li https://orcid.org/0000-0002-9110-6163
Alexander P. Ji https://orcid.org/0000-0002-4863-8842
Andrew B. Pace https://orcid.org/0000-0002-6021-8760
Denis Erkal  https://orcid.org/0000-0002-8448-5505
Sergey E. Koposov https://orcid.org/0000-0003-2644-135X
Nora Shipp  https://orcid.org/0000-0003-2497-091X
Gary S. Da Costa https://orcid.org/0000-0001-7019-649X
Lara R. Cullinane https://orcid.org/0000-0001-8536-0547
Kyler Kuehn  https://orcid.org/0000-0003-0120-0808
Geraint F. Lewis https://orcid.org/0000-0003-3081-9319
Dougal Mackey https://orcid.org/0000-0002-6529-8093
Jeffrey D. Simpson https://orcid.org/0000-0002-8165-2507
Daniel B. Zucker https://orcid.org/0000-0003-1124-8477
Peter S. Ferguson https://orcid.org/0000-0001-6957-1627
Sarah L. Martell https://orcid.org/0000-0002-3430-4163
Joss Bland-Hawthorn https://orcid.org/0000-0001-
Eduardo Balbinot https://orcid.org/0000-0002-1322-3153
```

Kiyan Tavangar https://orcid.org/0000-0001-6584-6144 Alex Drlica-Wagner https://orcid.org/0000-0001-Joshua D. Simon https://orcid.org/0000-0002-4733-4994

```
References
Astropy Collaboration, Robitaille, T. P., Tollerud, E. J., et al. 2013, A&A,
Astropy Collaboration, Price-Whelan, A. M., Sipőcz, B. M., et al. 2018, AJ,
   156, 123
Baumgardt, H., & Hilker, M. 2018, MNRAS, 478, 1520
Baumgardt, H., & Makino, J. 2003, MNRAS, 340, 227
Baumgardt, H., Parmentier, G., Gieles, M., & Vesperini, E. 2010, MNRAS,
Bechtol, K., Drlica-Wagner, A., Balbinot, E., et al. 2015, ApJ, 807, 50
Belokurov, V., Erkal, D., Evans, N. W., Koposov, S. E., & Deason, A. J. 2018,
      IRAS, 478, 611
Belokurov, V., Evans, N. W., Irwin, M. J., Hewett, P. C., & Wilkinson, M. I.
   2006, ApJL, 637, L29
Belokurov, V., & Koposov, S. E. 2016, MNRAS, 456, 602
Bernard, E. J., Ferguson, A. M. N., Schlafly, E. F., et al. 2014, MNRAS,
  443, L84
Blumenthal, G. R., Faber, S. M., Primack, J. R., & Rees, M. J. 1984, Natur,
   311, 517
Bonaca, A., Conroy, C., Price-Whelan, A. M., & Hogg, D. W. 2019, ApJL,
   881, L37
Bonaca, A., Geha, M., & Kallivayalil, N. 2012, ApJL, 760, L6
```

Bonaca, A., & Hogg, D. W. 2018, ApJ, 867, 101

Bonaca, A., Naidu, R. P., Conroy, C., et al. 2021, ApJL, 909, L26

```
415, L40
Boylan-Kolchin, M., Bullock, J. S., & Kaplinghat, M. 2012, MNRAS,
  422, 1203
Bullock, J. S., & Johnston, K. V. 2005, ApJ, 635, 931
Carlberg, R. G. 2009, ApJL, 705, L223
Carrera, R., Pancino, E., Gallart, C., & del Pino, A. 2013, MNRAS, 434, 1681
Casey, A. R., Da Costa, G., Keller, S. C., & Maunder, E. 2013, ApJ, 764, 39
Casey, A. R., Keller, S. C., Da Costa, G., Frebel, A., & Maunder, E. 2014, ApJ,
Chang, J., Yuan, Z., Xue, X.-X., et al. 2020, ApJ, 905, 100
Choi, J., Dotter, A., Conroy, C., et al. 2016, ApJ, 823, 102
Clementini, G., Ripepi, V., Molinaro, R., et al. 2019, A&A, 622, A60
Dehnen, W., & Binney, J. 1998, MNRAS, 294, 429
Drimmel, R., & Poggio, E. 2018, RNAAS, 2, 210
Drlica-Wagner, A., Bechtol, K., Rykoff, E. S., et al. 2015, ApJ, 813, 109
Erkal, D., Belokurov, V., Bovy, J., & Sanders, J. L. 2016a, MNRAS, 463, 102
Erkal, D., Sanders, J. L., & Belokurov, V. 2016b, MNRAS, 461, 1590
Erkal, D., Belokurov, V., Laporte, C. F. P., et al. 2019, MNRAS, 487, 2685
Errani, R., Penarrubia, J., & Tormen, G. 2015, MNRAS, 449, L46
Ferguson, P., Shipp, N., Drlica-Wagner, A., et al. 2022, AJ, 163, 18
Foreman-Mackey, D., Hogg, D. W., Lang, D., & Goodman, J. 2013, PASP,
Frebel, A., Lunnan, R., Casey, A. R., et al. 2013, ApJ, 771, 39
Freeman, K., & Bland-Hawthorn, J. 2002, ARA&A, 40, 487
Fritz, T. K., Battaglia, G., Pawlowski, M. S., et al. 2018, A&A, 619, A103
Fu, S. W., Simon, J. D., & Alarcón Jara, A. G. 2019, ApJ, 883, 11
Fu, S. W., Simon, J. D., Shetrone, M., et al. 2018, ApJ, 866, 42
Gaia Collaboration, Babusiaux, C., van Leeuwen, F., et al. 2018, A&A,
   616, A10
Gibbons, S. L. J., Belokurov, V., & Evans, N. W. 2014, MNRAS, 445, 3788
Gieles, M., Erkal, D., Antonini, F., Balbinot, E., & Peñarrubia, J. 2021, NatAs,
Gravity Collaboration, Abuter, R., Amorim, A., et al. 2018, A&A, 615, L15
Grillmair, C. J. 2006, ApJL, 645, L37
Grillmair, C. J., & Carlin, J. L 2016, in Tidal Streams in the Local Group and
   Beyond, ed. H. J. Newberg & J. L Carlin, Vol. 420 (Switzerland: Springer
   International), 87
Harris, W. E. 2010, arXiv:1012.3224
Hasselquist, S., Carlin, J. L., Holtzman, J. A., et al. 2019, ApJ, 872, 58
Helmi, A., Babusiaux, C., Koppelman, H. H., et al. 2018, Natur, 563, 85
Helmi, A., & White, S. D. M. 1999, MNRAS, 307, 495
Hernquist, L. 1990, ApJ, 356, 359
Holl, B., Audard, M., Nienartowicz, K., et al. 2018, A&A, 618, A30
Huang, K.-W., & Koposov, S. E. 2021, MNRAS, 500, 986
Hunter, J. D. 2007, CSE, 9, 90
Ibata, R., Malhan, K., Martin, N., et al. 2021, ApJ, 914, 123
Ibata, R. A., Lewis, G. F., Irwin, M. J., & Quinn, T. 2002, MNRAS, 332, 915
Ibata, R. A., Lewis, G. F., & Martin, N. F. 2016, ApJ, 819, 1
Ibata, R. A., Malhan, K., & Martin, N. F. 2019, ApJ, 872, 152
Ji, A. P., Li, T. S., Hansen, T. T., et al. 2020, AJ, 160, 181
Ji, A. P., Koposov, S. E., Li, T. S., et al. 2021, ApJ, 921, 32
Johnson, B. D., Conroy, C., Naidu, R. P., et al. 2020, ApJ, 900, 103
Johnston, K. V. 1998, ApJ, 495, 297
Johnston, K. V., Spergel, D. N., & Haydn, C. 2002, ApJ, 570, 656
Jones, E., Oliphant, T., Peterson, P., et al. 2001, SciPy: Open source scientific
   tools for Python, http://www.scipy.org/
Kallivayalil, N., van der Marel, R. P., Besla, G., Anderson, J., & Alcock, C.
   2013, ApJ, 764, 161
Kirby, E. N., Boylan-Kolchin, M., Cohen, J. G., et al. 2013a, ApJ, 770, 16
Kirby, E. N., Cohen, J. G., Guhathakurta, P., et al. 2013b, ApJ, 779, 102
Koposov, S., & Bartunov, O. 2006, in ASP Conf. Ser., 351, Astronomical Data
   Analysis Software and Systems XV, ed. C. Gabriel et al. (San Francisco,
   CA: ASP), 735
Koposov, S. E. 2019, RVSpecFit: Radial velocity and stellar atmospheric
   parameter fitting, Astrophysics Source Code Library, ascl:1907.013
Koposov, S. E., Belokurov, V., Torrealba, G., & Evans, N. W. 2015, ApJ,
Koposov, S. E., Rix, H.-W., & Hogg, D. W. 2010, ApJ, 712, 260
Koposov, S. E., Belokurov, V., Evans, N. W., et al. 2012, ApJ, 750, 80
Koposov, S. E., Belokurov, V., Li, T. S., et al. 2019, MNRAS, 485, 4726
Kruijssen, J. M. D. 2020, Natur, 583, 687
Küpper, A. H. W., Lane, R. R., & Heggie, D. C. 2012, MNRAS, 420, 2700
Kuzma, P. B., Da Costa, G. S., Keller, S. C., & Maunder, E. 2015, MNRAS,
   446, 3297
```

Bovy, J., Bahmanyar, A., Fritz, T. K., & Kallivayalil, N. 2016, ApJ, 833, 31 Boylan-Kolchin, M., Bullock, J. S., & Kaplinghat, M. 2011, MNRAS,

```
Kuzma, P. B., Da Costa, G. S., & Mackey, A. D. 2018, MNRAS, 473, 2881
Laevens, B. P. M., Martin, N. F., Bernard, E. J., et al. 2015, ApJ, 813, 44
Lamb, M. P., Venn, K. A., Shetrone, M. D., Sakari, C. M., & Pritzl, B. J. 2015,
   MNRAS, 448, 42
Lewis, I. J., Cannon, R. D., Taylor, K., et al. 2002, MNRAS, 333, 279
Li, G.-W., Yanny, B., Zhang, H.-T., et al. 2017a, RAA, 17, 062
Li, T. & S5 Collaboration 2021, Southern Stellar Stream Spectroscopic Survey:
   The First Public Data Release, Data Release 1, Zenodo, doi:10.5281/
   zenodo.4695135
Li, T. S., Simon, J. D., Drlica-Wagner, A., et al. 2017b, ApJ, 838, 8
Li, T. S., Koposov, S. E., Zucker, D. B., et al. 2019, MNRAS, 490, 3508
Li, T. S., Koposov, S. E., Erkal, D., et al. 2021, ApJ, 911, 149
Longeard, N., Martin, N., Ibata, R. A., et al. 2019, MNRAS, 490, 1498
Mackereth, J. T., Schiavon, R. P., Pfeffer, J., et al. 2019, MNRAS, 482, 3426
Majewski, S. R., Skrutskie, M. F., Weinberg, M. D., & Ostheimer, J. C. 2003,
    ApJ, 599, 1082
Malhan, K., Valluri, M., & Freese, K. 2021a, MNRAS, 501, 179
Malhan, K., Yuan, Z., Ibata, R., et al. 2021b, ApJ, 920, 51
Martin, C., Carlin, J. L., Newberg, H. J., & Grillmair, C. 2013, ApJL, 765, L39
Massari, D., Koppelman, H. H., & Helmi, A. 2019, A&A, 630, L4
Mateu, C., Read, J. I., & Kawata, D. 2018, MNRAS, 474, 4112
McMillan, P. J. 2017, MNRAS, 465, 76
Muraveva, T., Delgado, H. E., Clementini, G., Sarro, L. M., & Garofalo, A.
  2018, MNRAS, 481, 1195
Naidu, R. P., Conroy, C., Bonaca, A., et al. 2020, ApJ, 901, 48
Naidu, R. P., Conroy, C., Bonaca, A., et al. 2021, ApJ, 923, 92
Newberg, H. J., Willett, B. A., Yanny, B., & Xu, Y. 2010, ApJ, 711, 32
Newberg, H. J., Yanny, B., & Willett, B. A. 2009, ApJ, 700, L61
Norris, J. E., Wyse, R. F. G., Gilmore, G., et al. 2010, ApJ, 723, 1632
Odenkirchen, M., Grebel, E. K., Kayser, A., Rix, H.-W., & Dehnen, W. 2009,
    J, 137, 3378
Panithanpaisal, N., Sanderson, R. E., Wetzel, A., et al. 2021, ApJ, 920, 10
Pawlowski, M. S., & Kroupa, P. 2013, MNRAS, 435, 2116
Pawlowski, M. S., McGaugh, S. S., & Jerjen, H. 2015, MNRAS, 453, 1047
Pawlowski, M. S., Pflamm-Altenburg, J., & Kroupa, P. 2012, MNRAS,
   423, 1109
Peebles, P. J. E. 1965, ApJ, 142, 1317
Pietrzyński, G., Graczyk, D., Gieren, W., et al. 2013, Natur, 495, 76
```

```
Press, W. H., & Schechter, P. 1974, ApJ, 187, 425
Price-Whelan, A., Sipőcz, B., Lenz, D., et al. 2020, adrn/gala: v1.3, Zenodo,
  doi:10.5281/zenodo.4159870
Price-Whelan, A. M. 2017, JOSS, 2, 388
Reid, M. J., & Brunthaler, A. 2004, ApJ, 616, 872
Riello, M., De Angeli, F., Evans, D. W., et al. 2021, A&A, 649, A3
Riley, A. H., & Strigari, L. E. 2020, MNRAS, 494, 983
Roederer, I. U., Mateo, M., Bailey, J. I., et al. 2016, MNRAS, 455, 2417
Schlafly, E. F., & Finkbeiner, D. P. 2011, ApJ, 737, 103
Schlegel, D. J., Finkbeiner, D. P., & Davis, M. 1998, ApJ, 500, 525
Searle, L., & Zinn, R. 1978, ApJ, 225, 357
Sesar, B., Bovy, J., Bernard, E. J., et al. 2015, ApJ, 809, 59
Sharp, R., Saunders, W., Smith, G., et al. 2006, Proc. SPIE, 6269, 62690G
Shipp, N., Drlica-Wagner, A., Balbinot, E., et al. 2018, ApJ, 862, 114
Shipp, N., Li, T. S., Pace, A. B., et al. 2019, ApJ, 885, 3
Shipp, N., Erkal, D., Drlica-Wagner, A., et al. 2021, ApJ, 923, 149
Simon, J. D. 2018, ApJ, 863, 89
Simon, J. D. 2019, ARA&A, 57, 375
Simon, J. D., Geha, M., Minor, Q. E., et al. 2011, ApJ, 733, 46
Simon, J. D., Li, T. S., Drlica-Wagner, A., et al. 2017, ApJ, 838, 11
van der Marel, R. P., Alves, D. R., Hardy, E., & Suntzeff, N. B. 2002, AJ,
van der Marel, R. P., & Kallivayalil, N. 2014, ApJ, 781, 121
van der Walt, S., Colbert, S. C., & Varoquaux, G. 2011, CSE, 13, 22
Varghese, A., Ibata, R., & Lewis, G. F. 2011, MNRAS, 417, 198
Vasiliev, E., & Baumgardt, H. 2021, MNRAS, 505, 5978
Vasiliev, E., Belokurov, V., & Evans, W. 2022, ApJ, 926, 203
Walker, M. G., Mateo, M., Olszewski, E. W., et al. 2007, ApJL, 667, L53
Wan, Z., Lewis, G. F., Li, T. S., et al. 2020, Natur, 583, 768
Waskom, M., Botvinnik, O., & drewokane, O. 2016, Seaborn: V0.7.0 (January
  2016), v0.7.0, Zenodo, doi:10.5281/zenodo.45133
Wenger, M., Ochsenbein, F., Egret, D., et al. 2000, A&AS, 143, 9
Yam, W., Carlin, J. L., Newberg, H. J., et al. 2013, ApJ, 776, 133
Yang, C., Xue, X.-X., Li, J., et al. 2019, ApJ, 886, 154
Yuan, Z., Chang, J., Beers, T. C., & Huang, Y. 2020, ApJL, 898, L37
Yuan, Z., Smith, M. C., Xue, X.-X., et al. 2019, ApJ, 881, 164
Yuan, Z., Malhan, K., Sestito, F., et al. 2021, arXiv:2112.05775
```